1 Observed change (northern hemisphere)

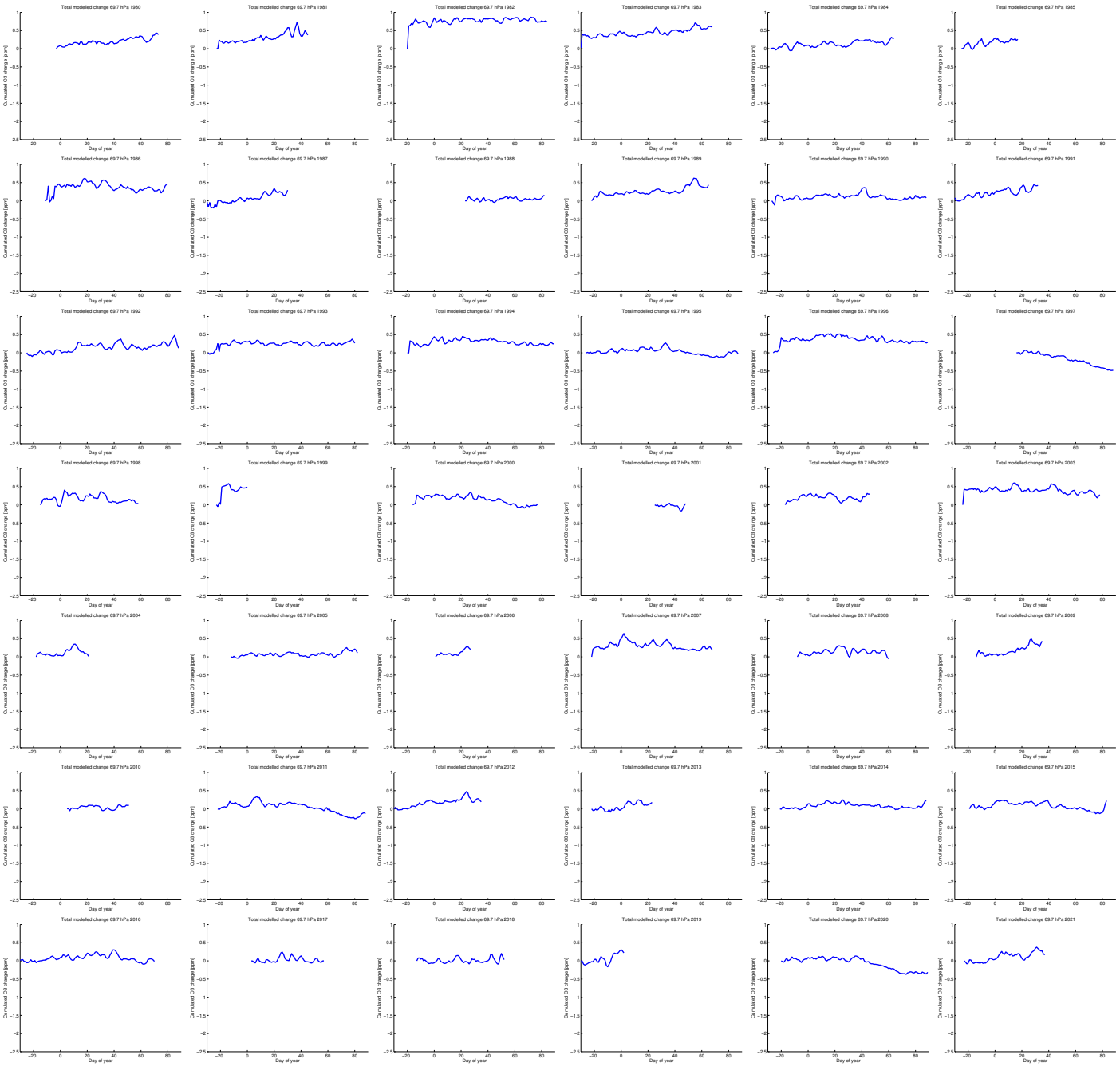

Figure S1: Cumulated total change of vortex-averaged ozone mixing ratio for the northern hemispheric winters 1979/1980–2020/2021 at 70 hPa (layer 1) simulated by ATLAS-SWIFT as a function of the day of year (cf. Figure 1 of the main manuscript).

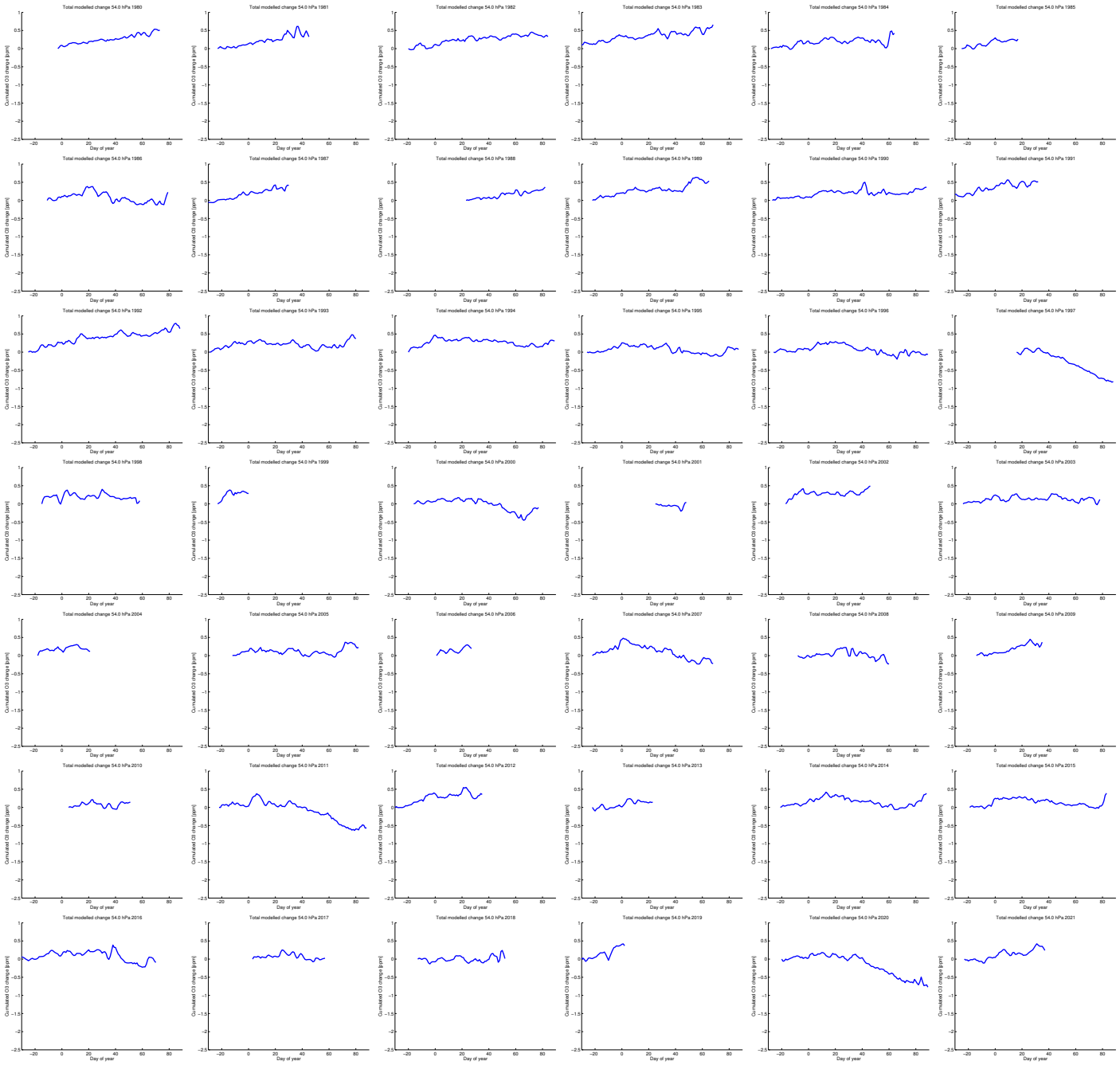

Figure S2: Cumulated total change of vortex-averaged ozone mixing ratio for the northern hemispheric winters 1979/1980–2020/2021 at 54 hPa (layer 2) simulated by ATLAS-SWIFT as a function of the day of year (cf. Figure 1 of the main manuscript).

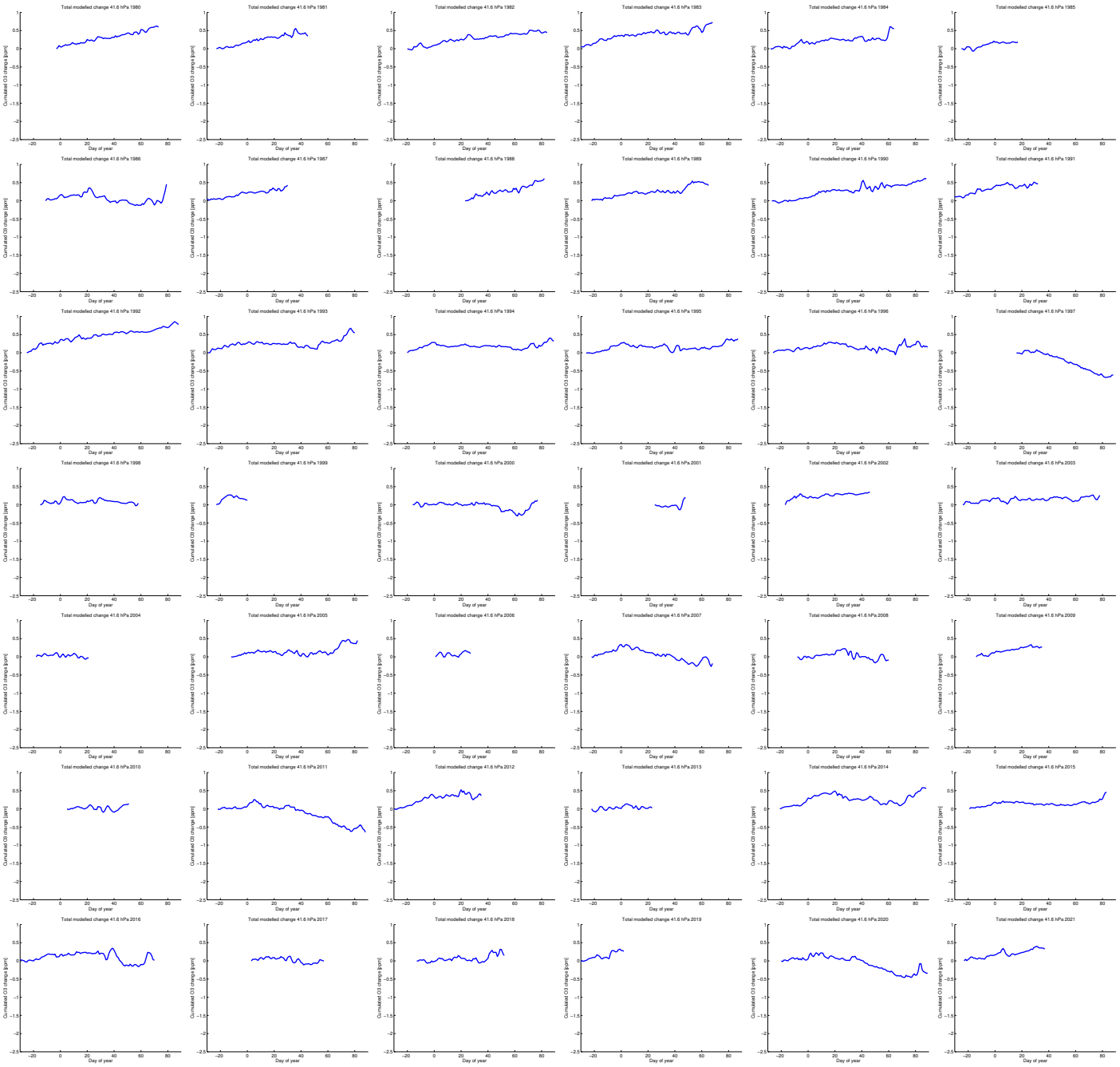

Figure S3: Cumulated total change of vortex-averaged ozone mixing ratio for the northern hemispheric winters 1979/1980–2020/2021 at 42 hPa (layer 3) simulated by ATLAS-SWIFT as a function of the day of year (cf. Figure 1 of the main manuscript).

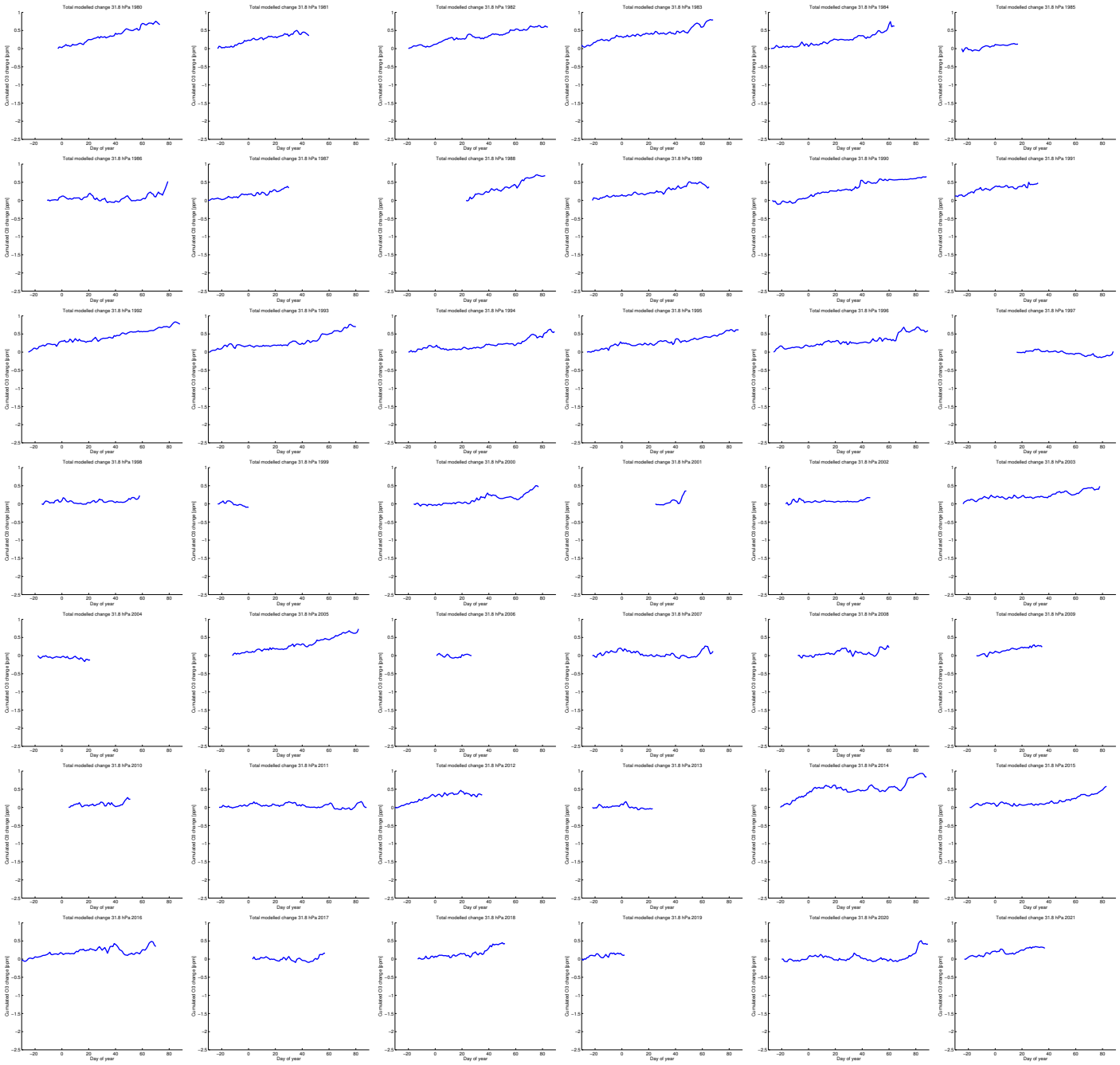

Figure S4: Cumulated total change of vortex-averaged ozone mixing ratio for the northern hemispheric winters 1979/1980–2020/2021 at 32 hPa (layer 4) simulated by ATLAS-SWIFT as a function of the day of year (cf. Figure 1 of the main manuscript).

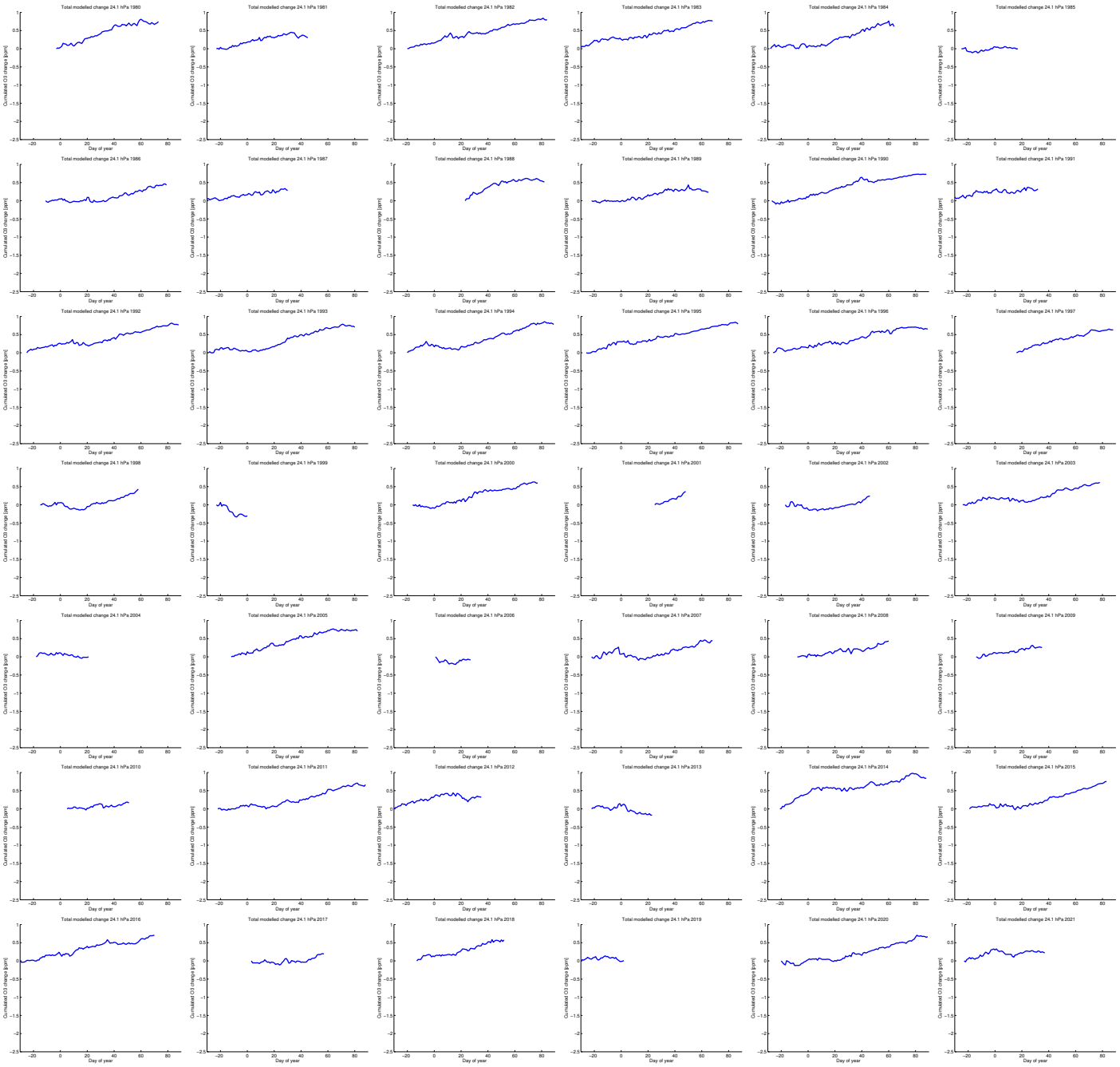

Figure S5: Cumulated total change of vortex-averaged ozone mixing ratio for the northern hemispheric winters 1979/1980–2020/2021 at 24 hPa (layer 5) simulated by ATLAS-SWIFT as a function of the day of year (cf. Figure 1 of the main manuscript).

2 Chemical change (northern hemisphere)

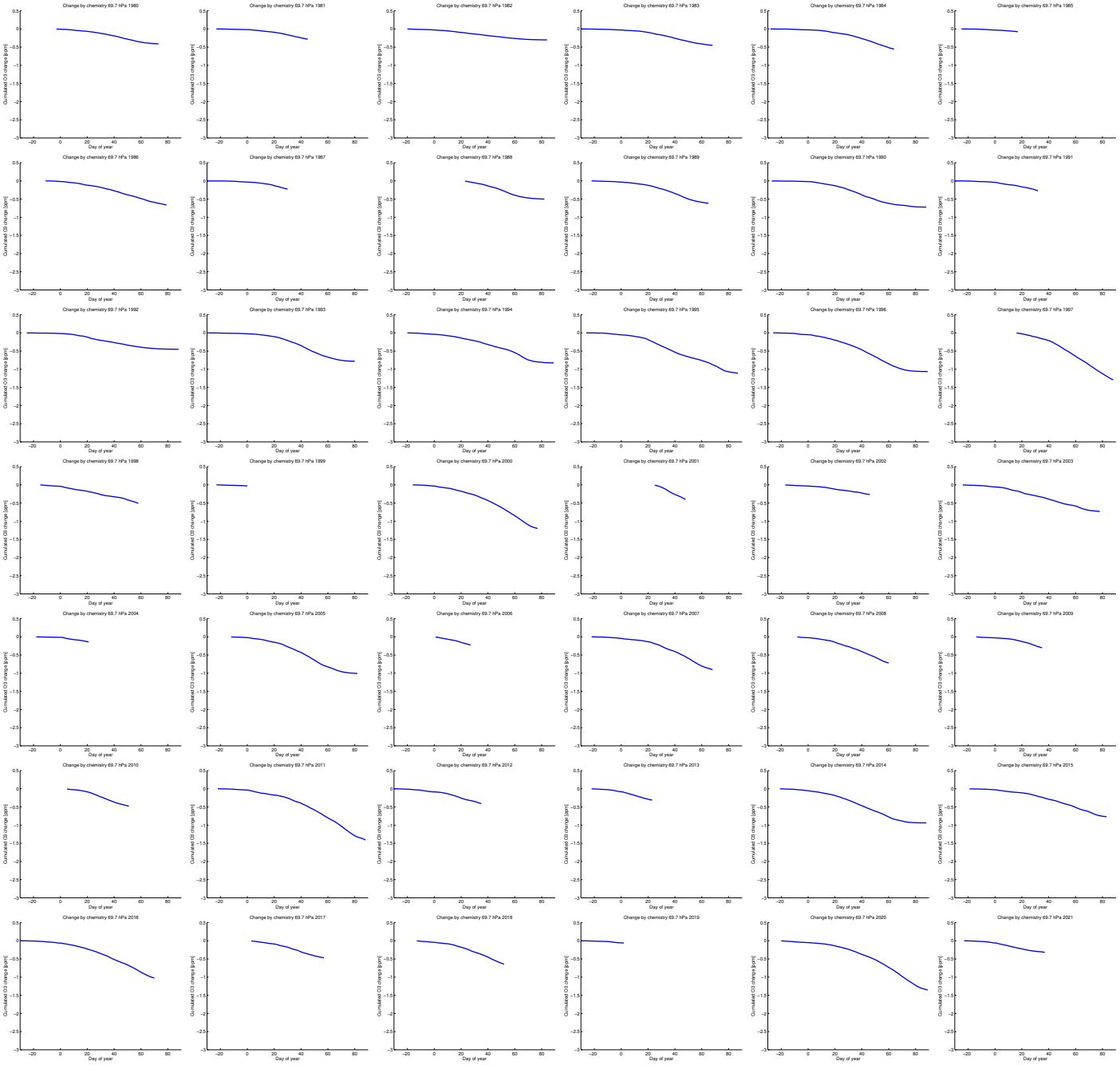

Figure S6: Cumulated change by chemistry of vortex-averaged ozone mixing ratio for the northern hemispheric winters 1979/1980–2020/2021 at 70 hPa (layer 1) simulated by ATLAS-SWIFT as a function of the day of year (cf. Figure 1 of the main manuscript).

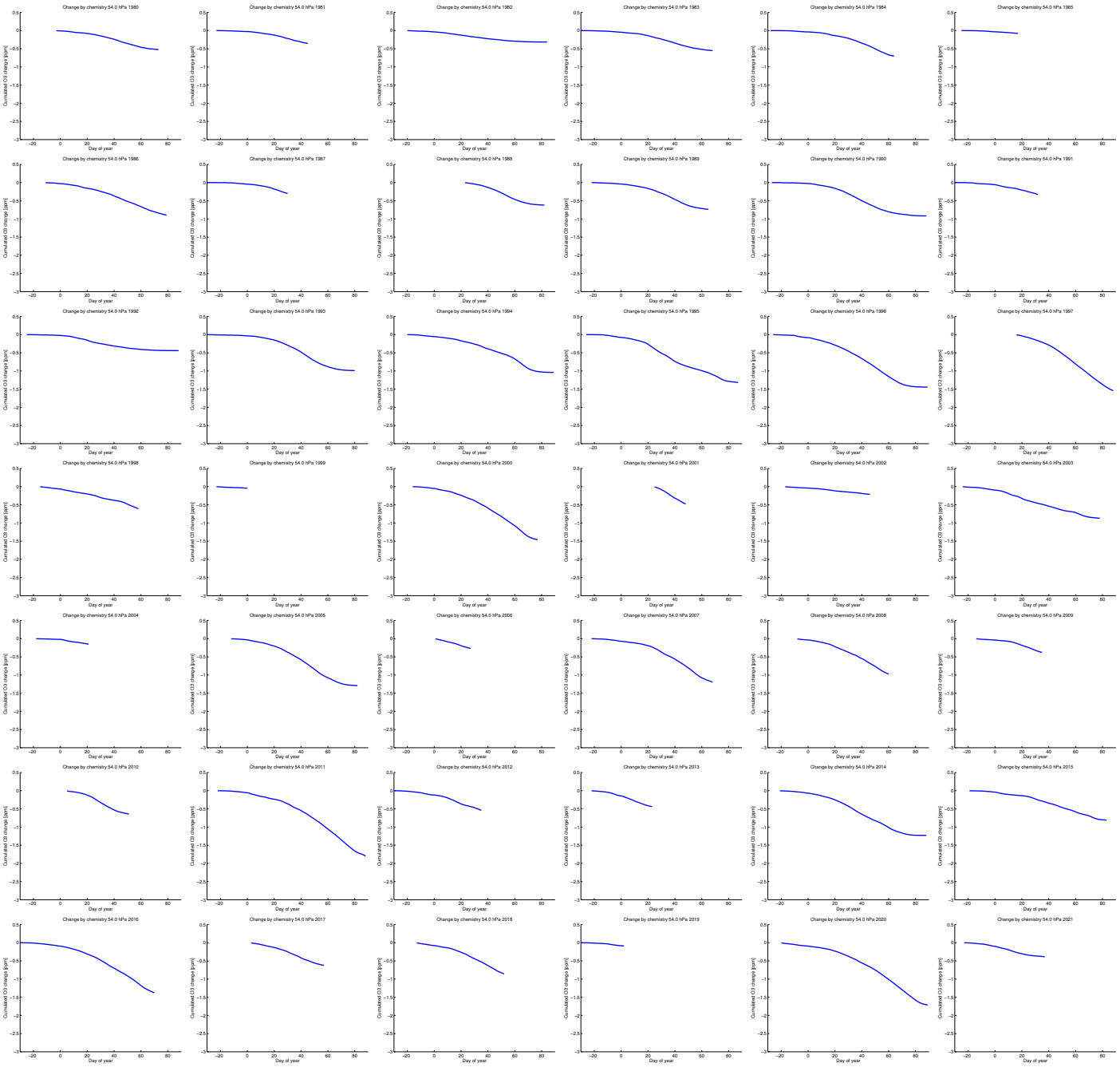

Figure S7: Cumulated change by chemistry of vortex-averaged ozone mixing ratio for the northern hemispheric winters 1979/1980–2020/2021 at 54 hPa (layer 2) simulated by ATLAS-SWIFT as a function of the day of year (cf. Figure 1 of the main manuscript).

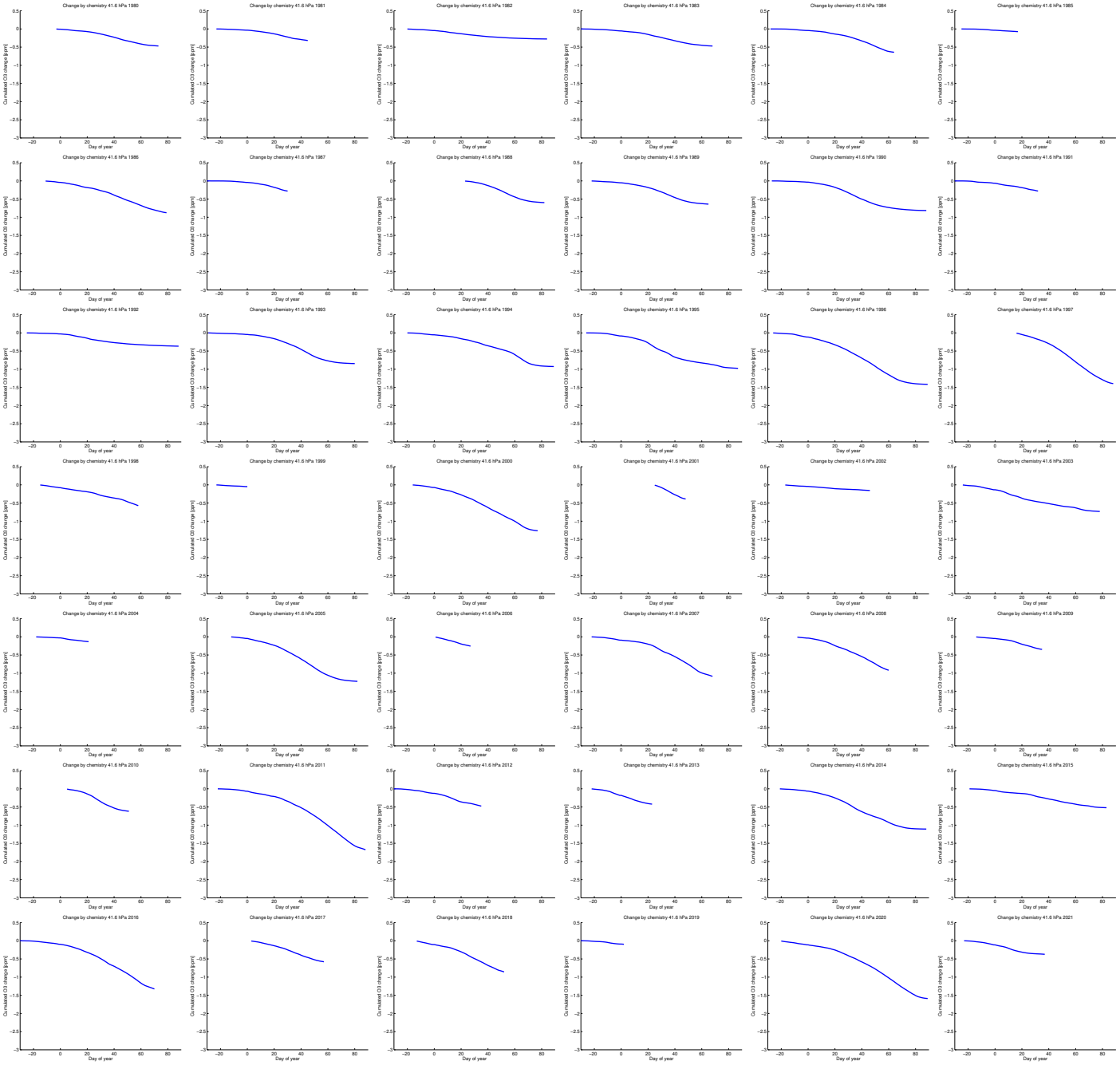

Figure S8: Cumulated change by chemistry of vortex-averaged ozone mixing ratio for the northern hemispheric winters 1979/1980–2020/2021 at 42 hPa (layer 3) simulated by ATLAS-SWIFT as a function of the day of year (cf. Figure 1 of the main manuscript).

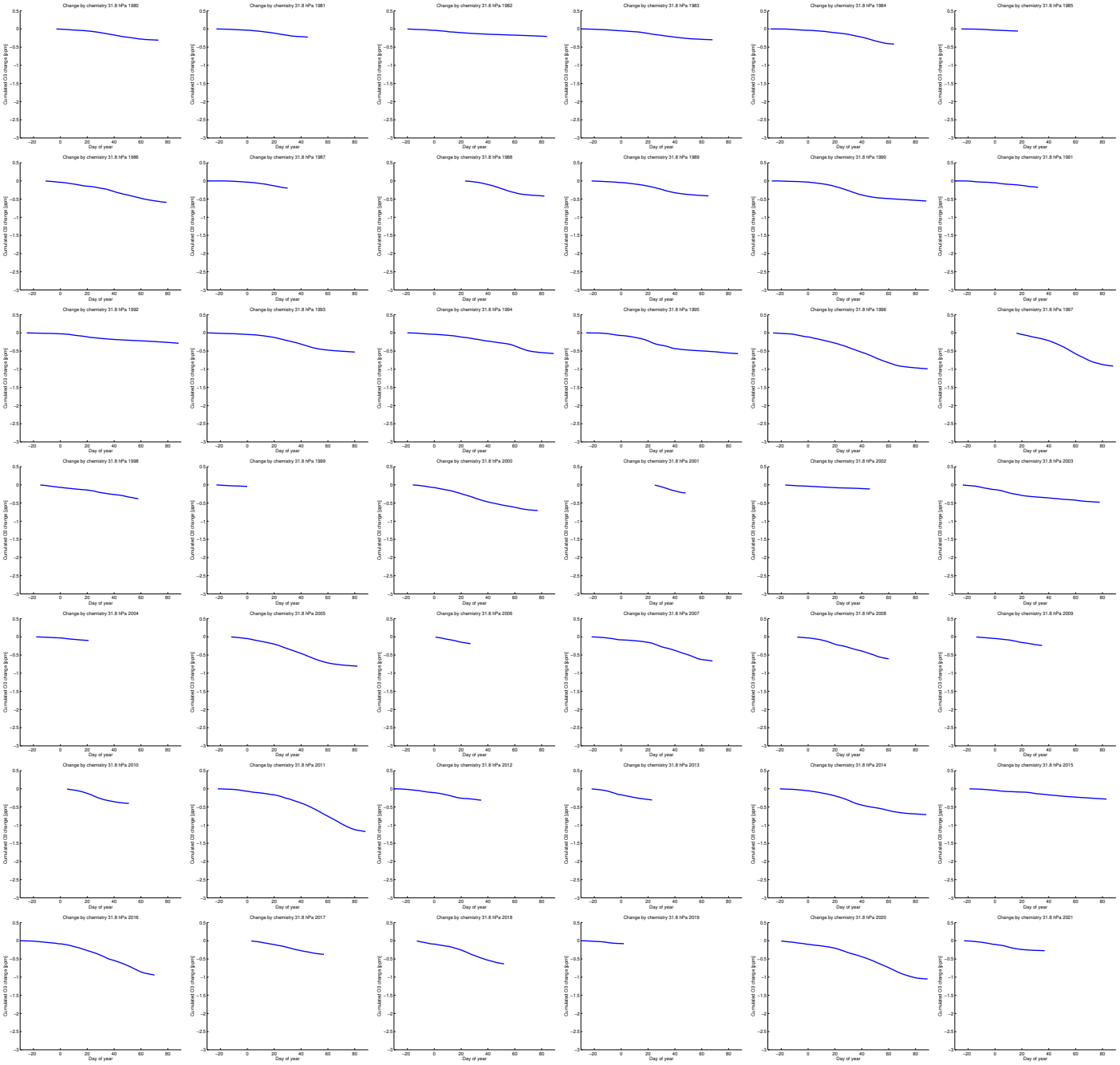

Figure S9: Cumulated change by chemistry of vortex-averaged ozone mixing ratio for the northern hemispheric winters 1979/1980–2020/2021 at 32 hPa (layer 4) simulated by ATLAS-SWIFT as a function of the day of year (cf. Figure 1 of the main manuscript).

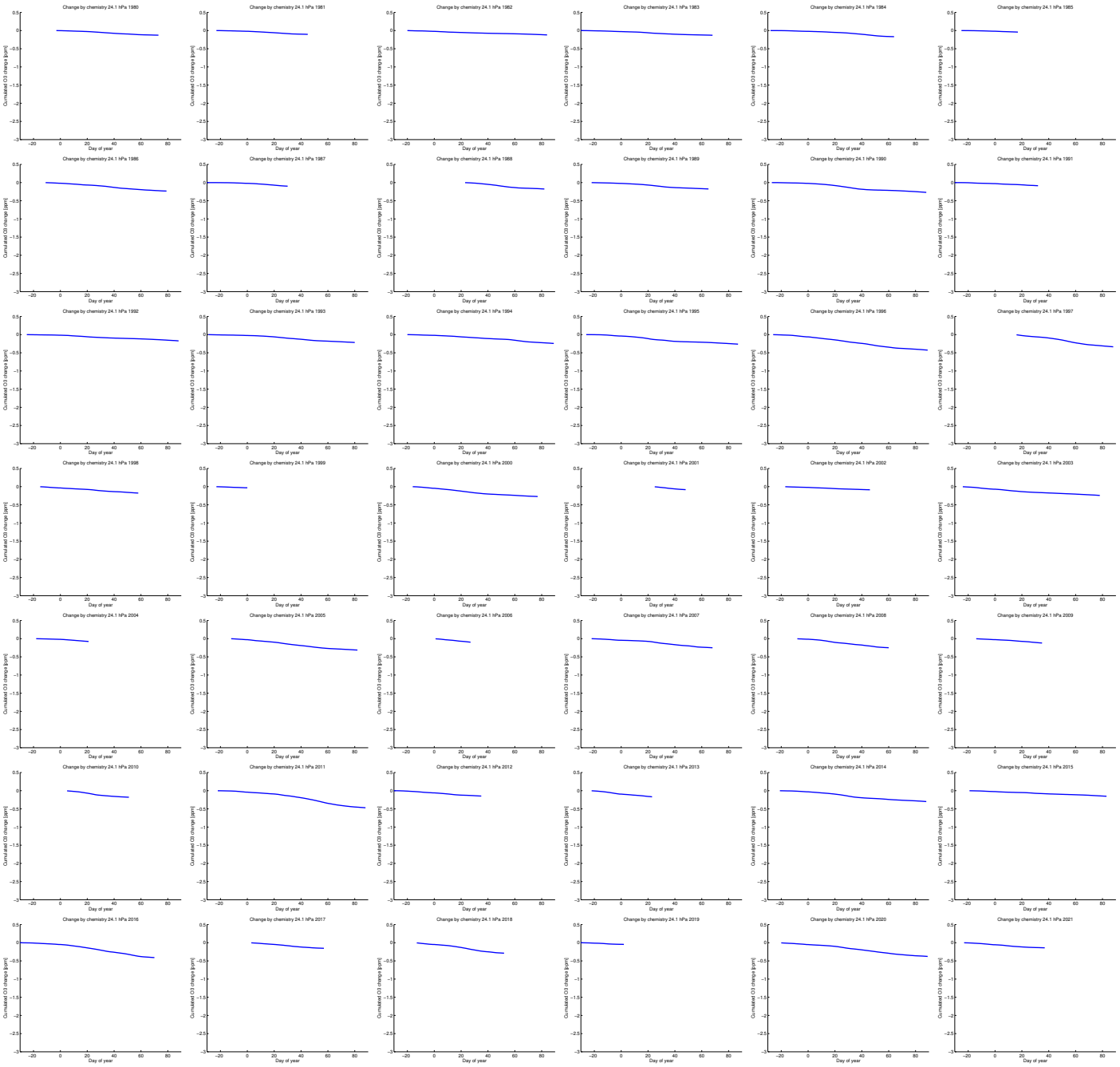

Figure S10: Cumulated change by chemistry of vortex-averaged ozone mixing ratio for the northern hemispheric winters 1979/1980–2020/2021 at 24 hPa (layer 5) simulated by ATLAS-SWIFT as a function of the day of year (cf. Figure 1 of the main manuscript).

3 Transport change and fit for constant term (northern hemisphere)

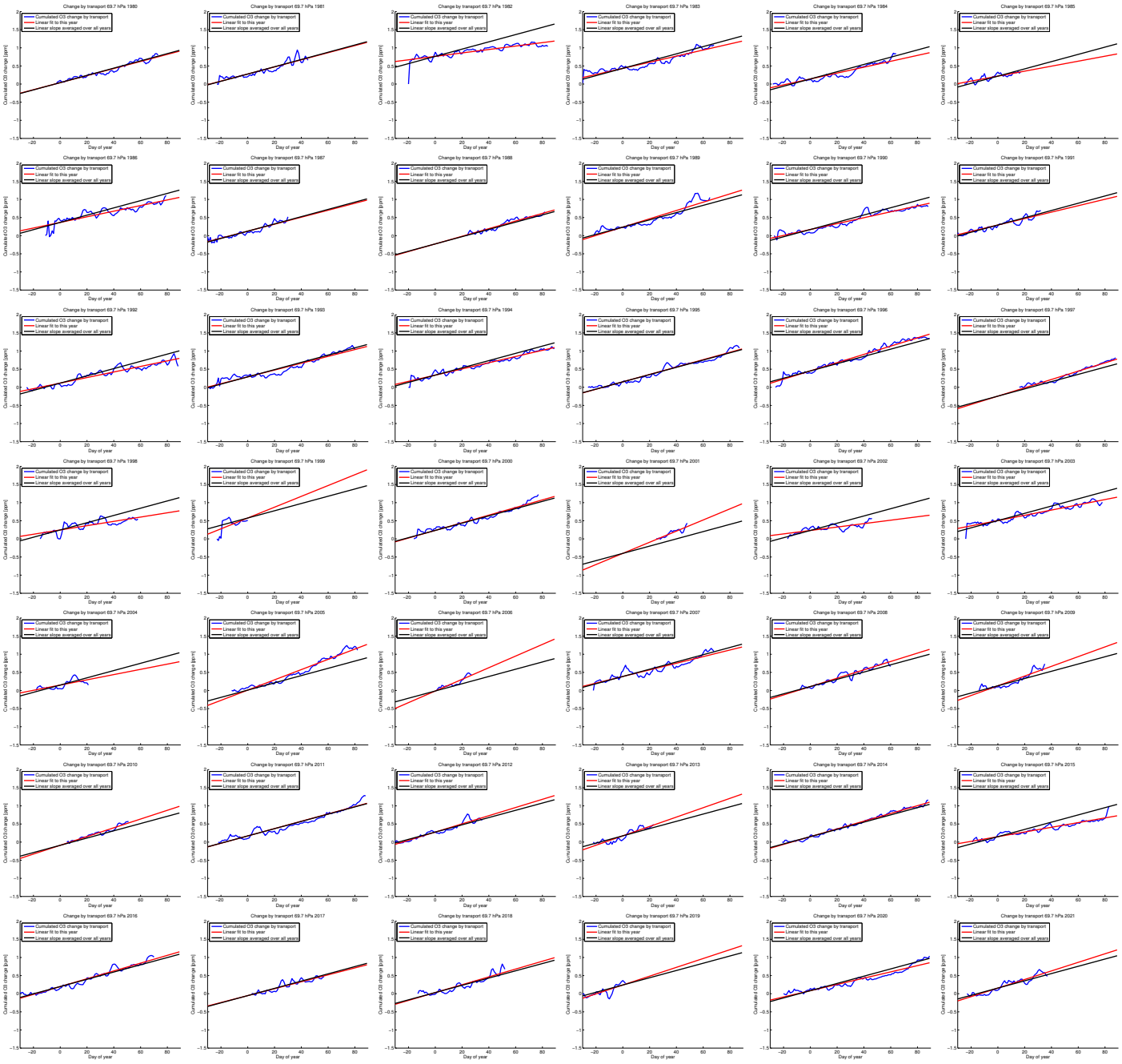

Figure S11: Cumulated change by transport of vortex-averaged ozone mixing ratio for the northern hemispheric winters 1979/1980–2020/2021 at 70 hPa (layer 1) simulated by ATLAS-SWIFT as a function of the day of year (blue), linear fit to the cumulated change (red) and linear slope based on the averaged slope of the fits of all years (black) (cf. Figure 1 and 2 of the main manuscript).

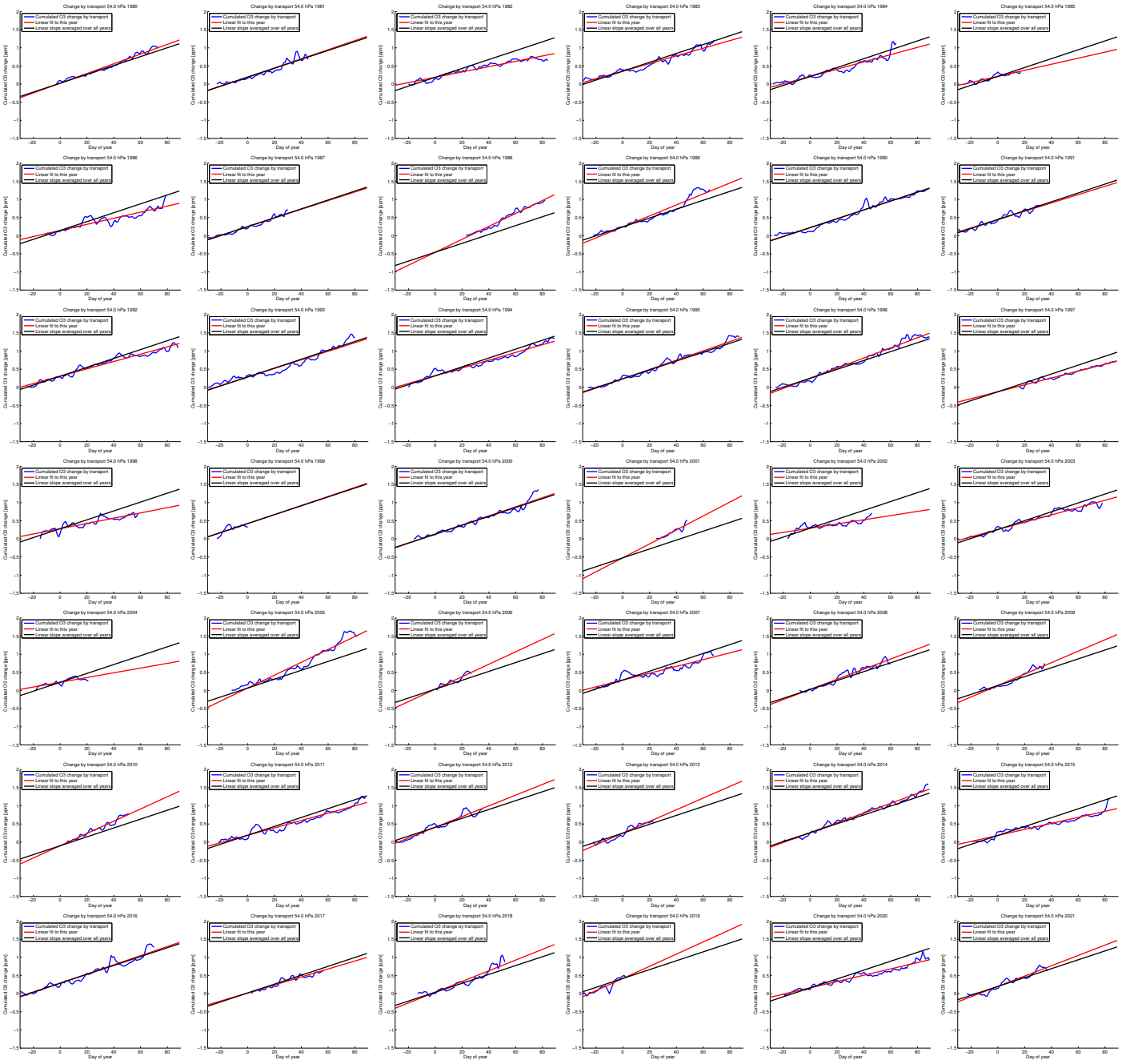

Figure S12: Cumulated change by transport of vortex-averaged ozone mixing ratio for the northern hemispheric winters 1979/1980–2020/2021 at 54 hPa (layer 2) simulated by ATLAS-SWIFT as a function of the day of year (blue), linear fit to the cumulated change (red) and linear slope based on the averaged slope of the fits of all years (black) (cf. Figure 1 and 2 of the main manuscript).

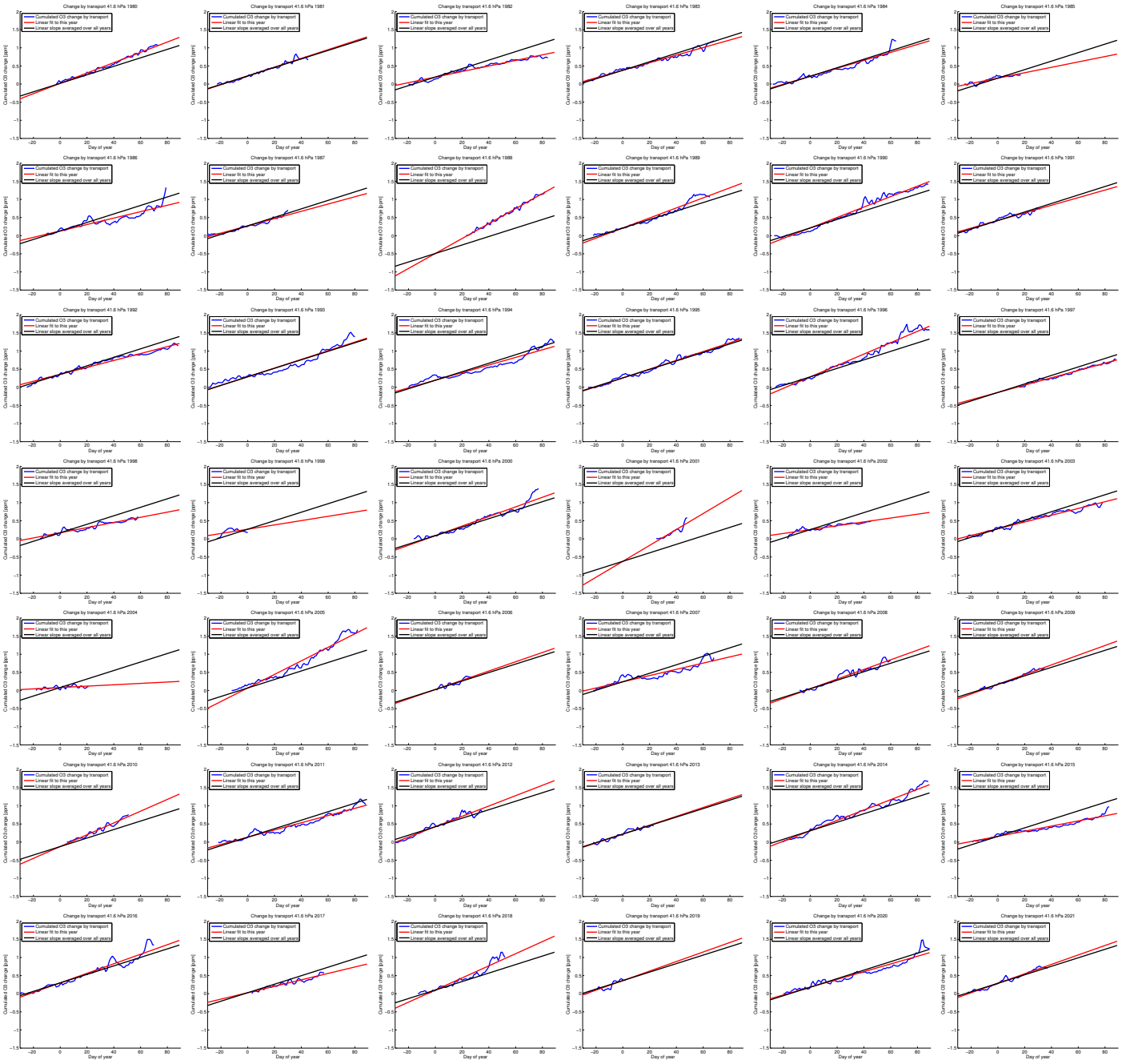

Figure S13: Cumulated change by transport of vortex-averaged ozone mixing ratio for the northern hemispheric winters 1979/1980–2020/2021 at 42 hPa (layer 3) simulated by ATLAS-SWIFT as a function of the day of year (blue), linear fit to the cumulated change (red) and linear slope based on the averaged slope of the fits of all years (black) (cf. Figure 1 and 2 of the main manuscript).

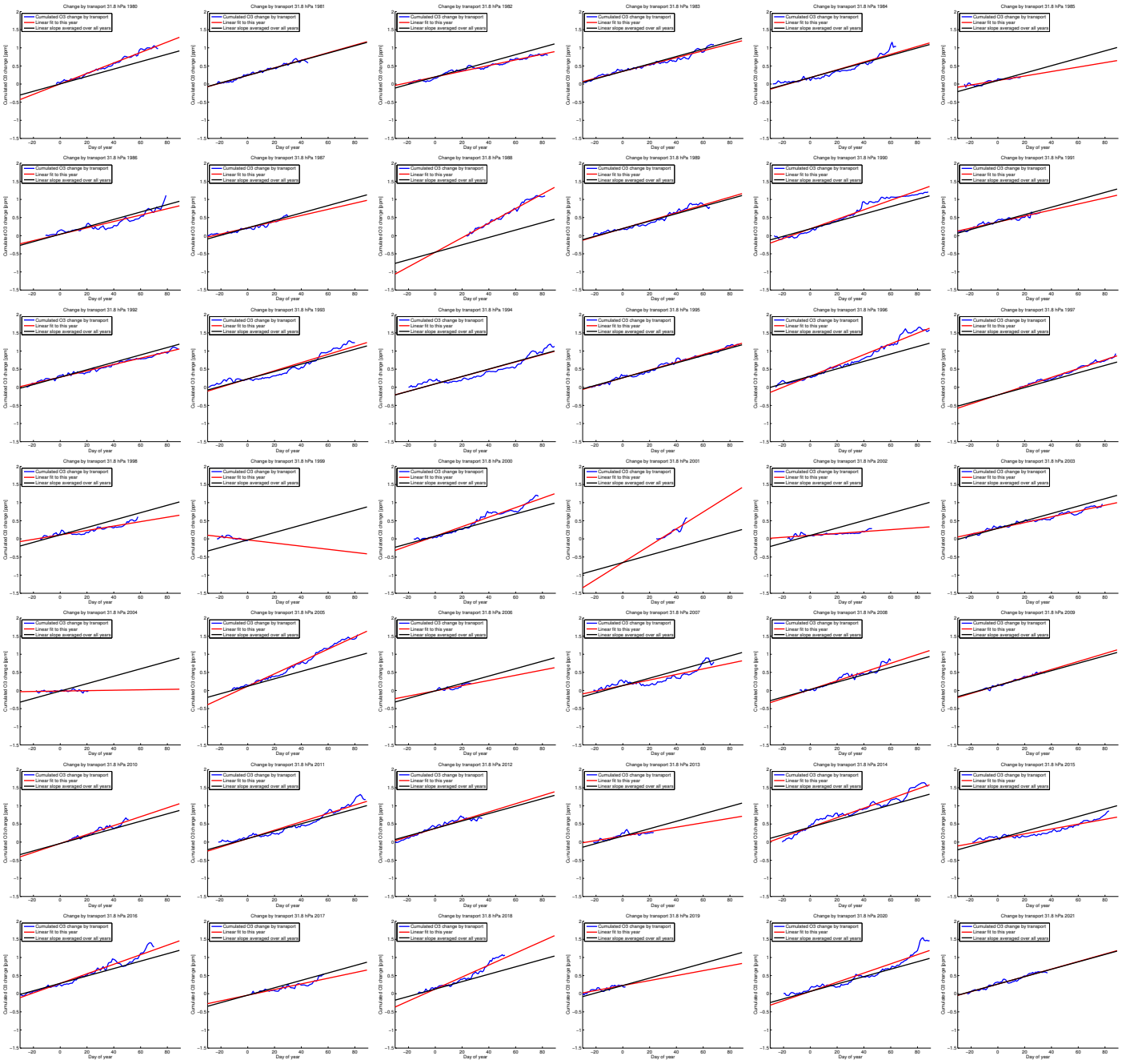

Figure S14: Cumulated change by transport of vortex-averaged ozone mixing ratio for the northern hemispheric winters 1979/1980–2020/2021 at 32 hPa (layer 4) simulated by ATLAS-SWIFT as a function of the day of year (blue), linear fit to the cumulated change (red) and linear slope based on the averaged slope of the fits of all years (black) (cf. Figure 1 and 2 of the main manuscript).

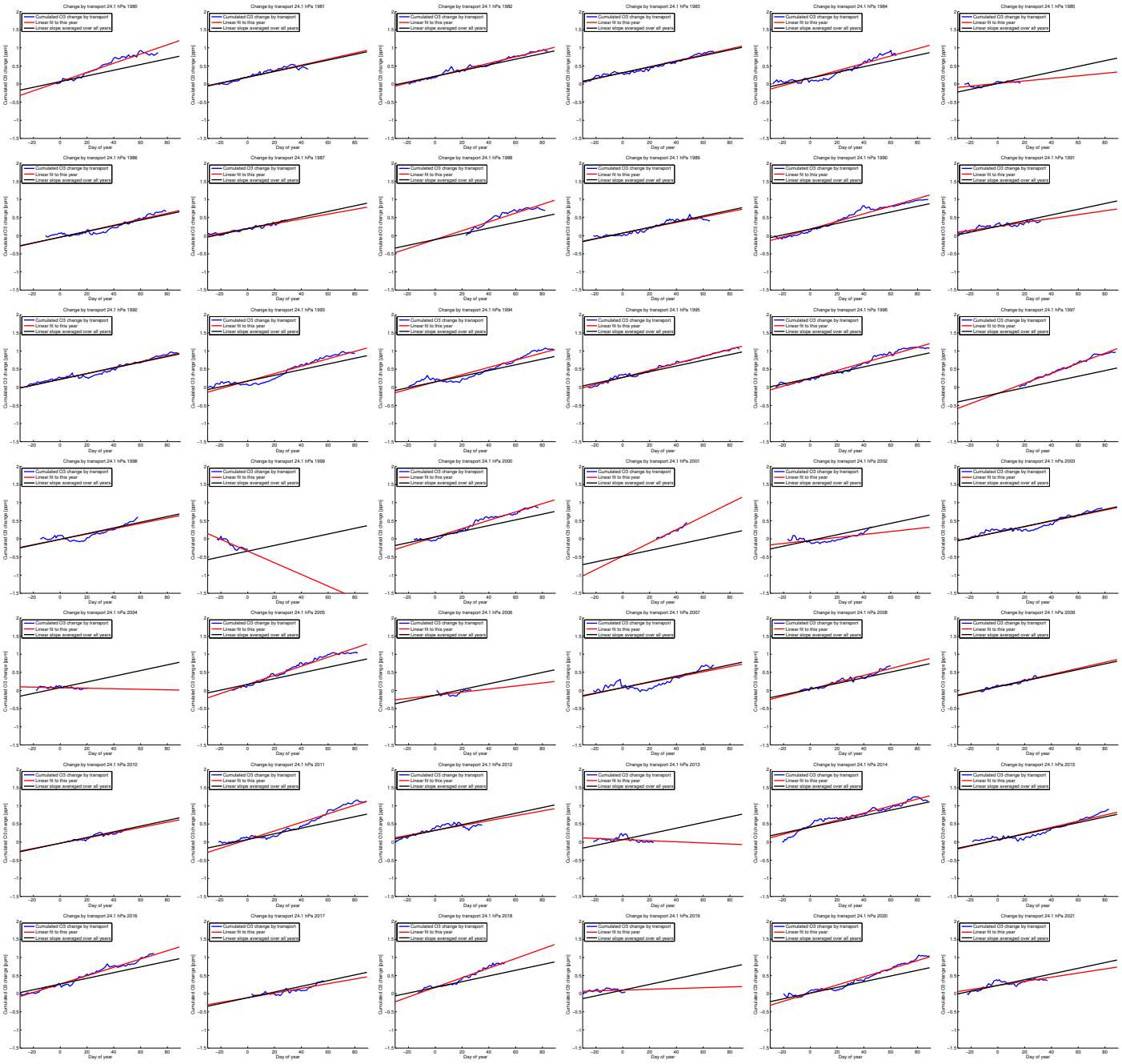

Figure S15: Cumulated change by transport of vortex-averaged ozone mixing ratio for the northern hemispheric winters 1979/1980–2020/2021 at 24 hPa (layer 5) simulated by ATLAS-SWIFT as a function of the day of year (blue), linear fit to the cumulated change (red) and linear slope based on the averaged slope of the fits of all years (black) (cf. Figure 1 and 2 of the main manuscript).

4 Fit for temperature-dependent term (northern hemisphere)

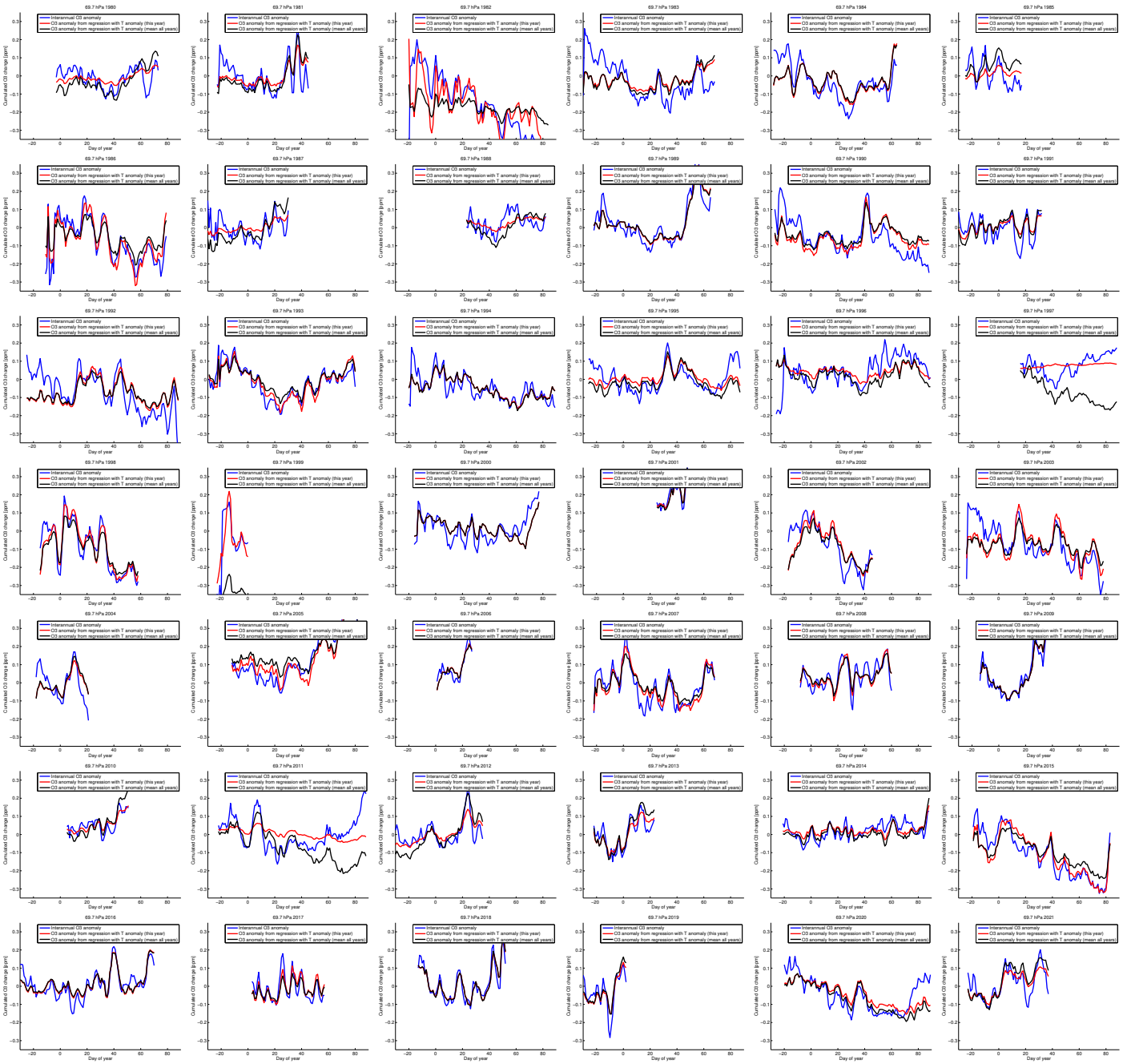

Figure S16: Anomaly of the cumulated vortex-averaged ozone change by transport at 70 hPa (layer 1) for the northern hemispheric winters 1979/1980–2020/2021 (blue, after subtraction of the change by transport that is constant in every year), vortex-averaged temperatures of the individual years regressed on the ozone anomaly (red) and vortex-averaged temperatures scaled by the mean slope of the regressions of all years (black) (cf. Figure 3 of the main manuscript).

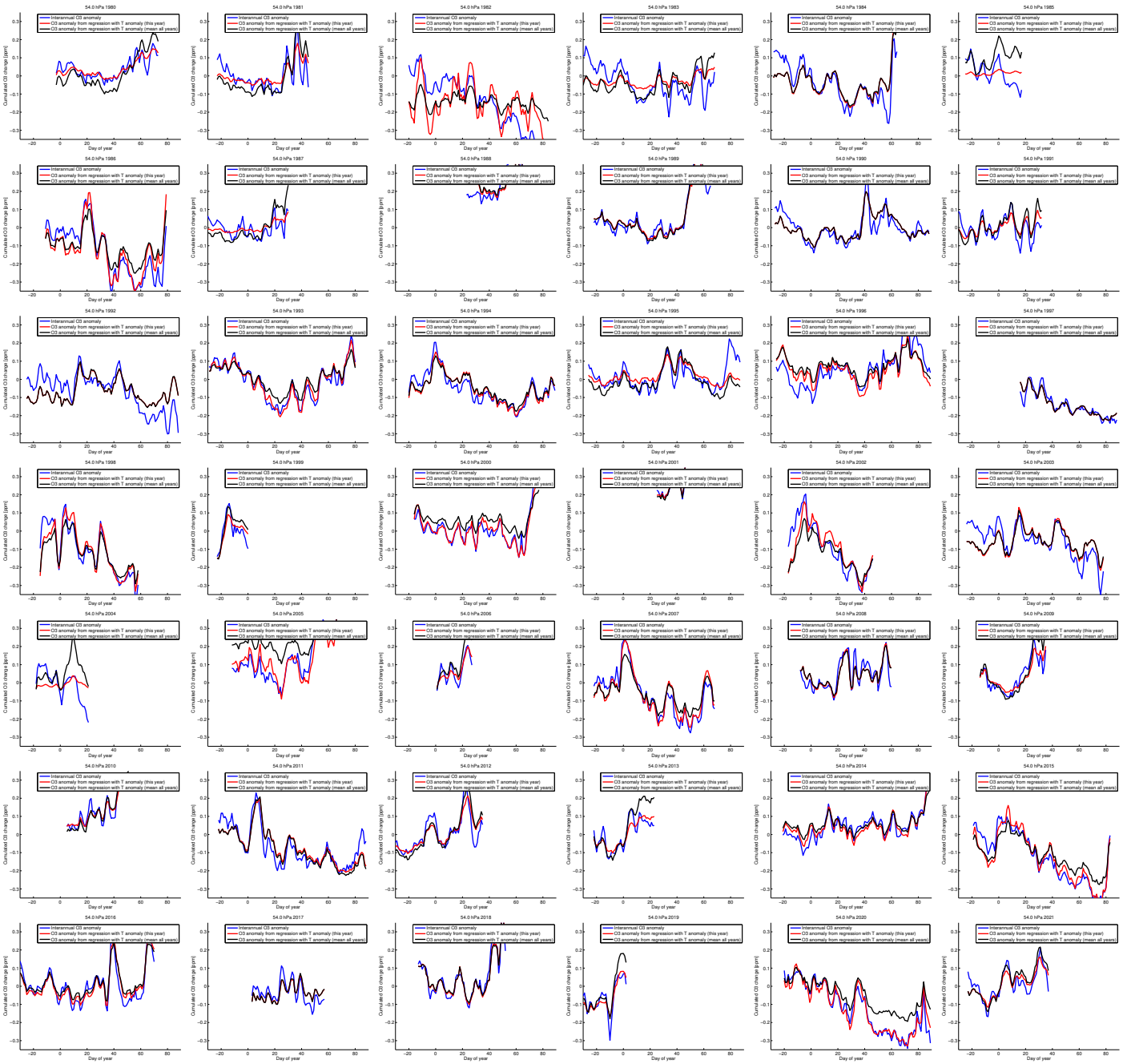

Figure S17: Anomaly of the cumulated vortex-averaged ozone change by transport at 54 hPa (layer 2) for the northern hemispheric winters 1979/1980–2020/2021 (blue, after subtraction of the change by transport that is constant in every year), vortex-averaged temperatures of the individual years regressed on the ozone anomaly (red) and vortex-averaged temperatures scaled by the mean slope of the regressions of all years (black) (cf. Figure 3 of the main manuscript).

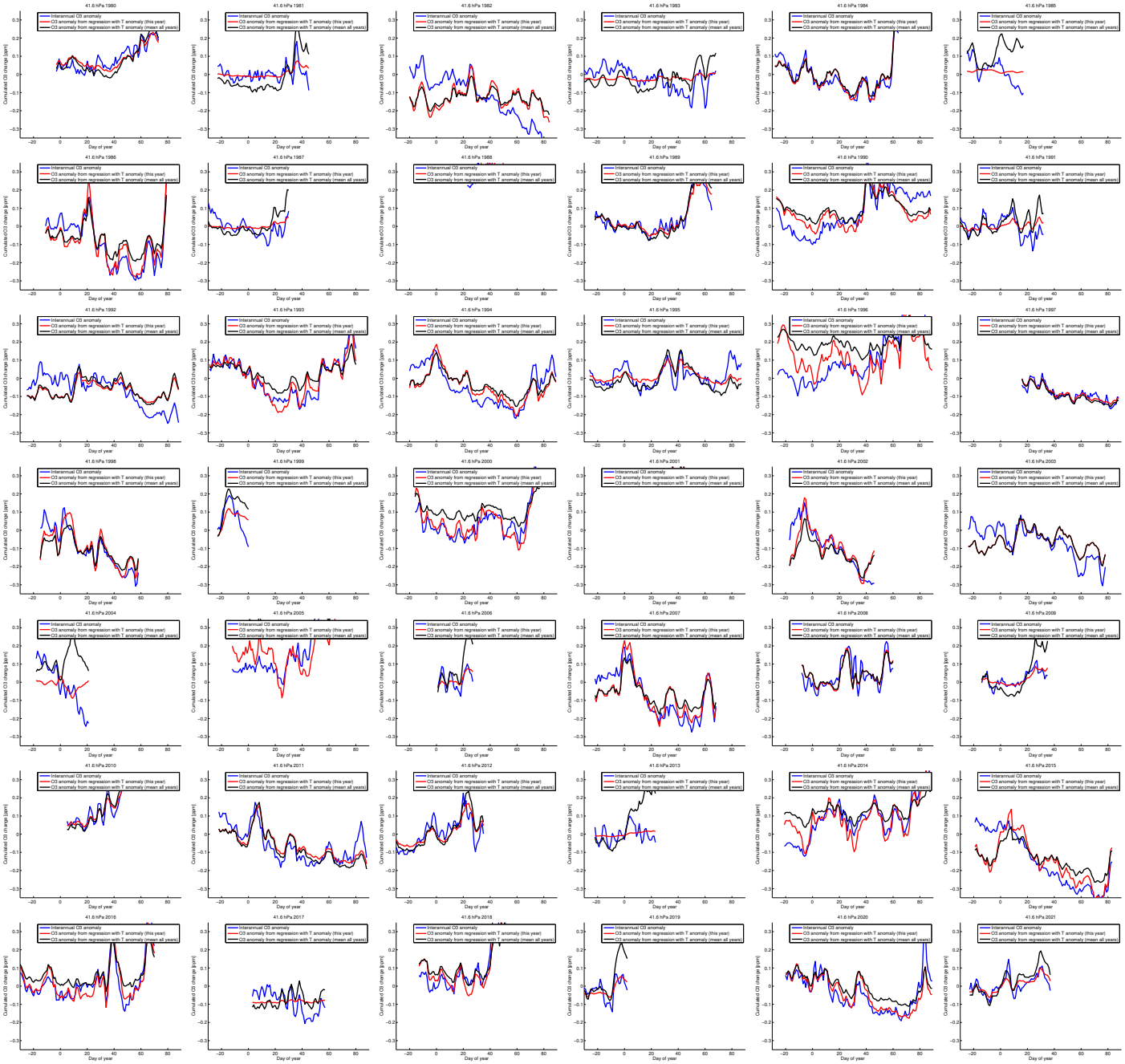

Figure S18: Anomaly of the cumulated vortex-averaged ozone change by transport at 42 hPa (layer 3) for the northern hemispheric winters 1979/1980–2020/2021 (blue, after subtraction of the change by transport that is constant in every year), vortex-averaged temperatures of the individual years regressed on the ozone anomaly (red) and vortex-averaged temperatures scaled by the mean slope of the regressions of all years (black) (cf. Figure 3 of the main manuscript).

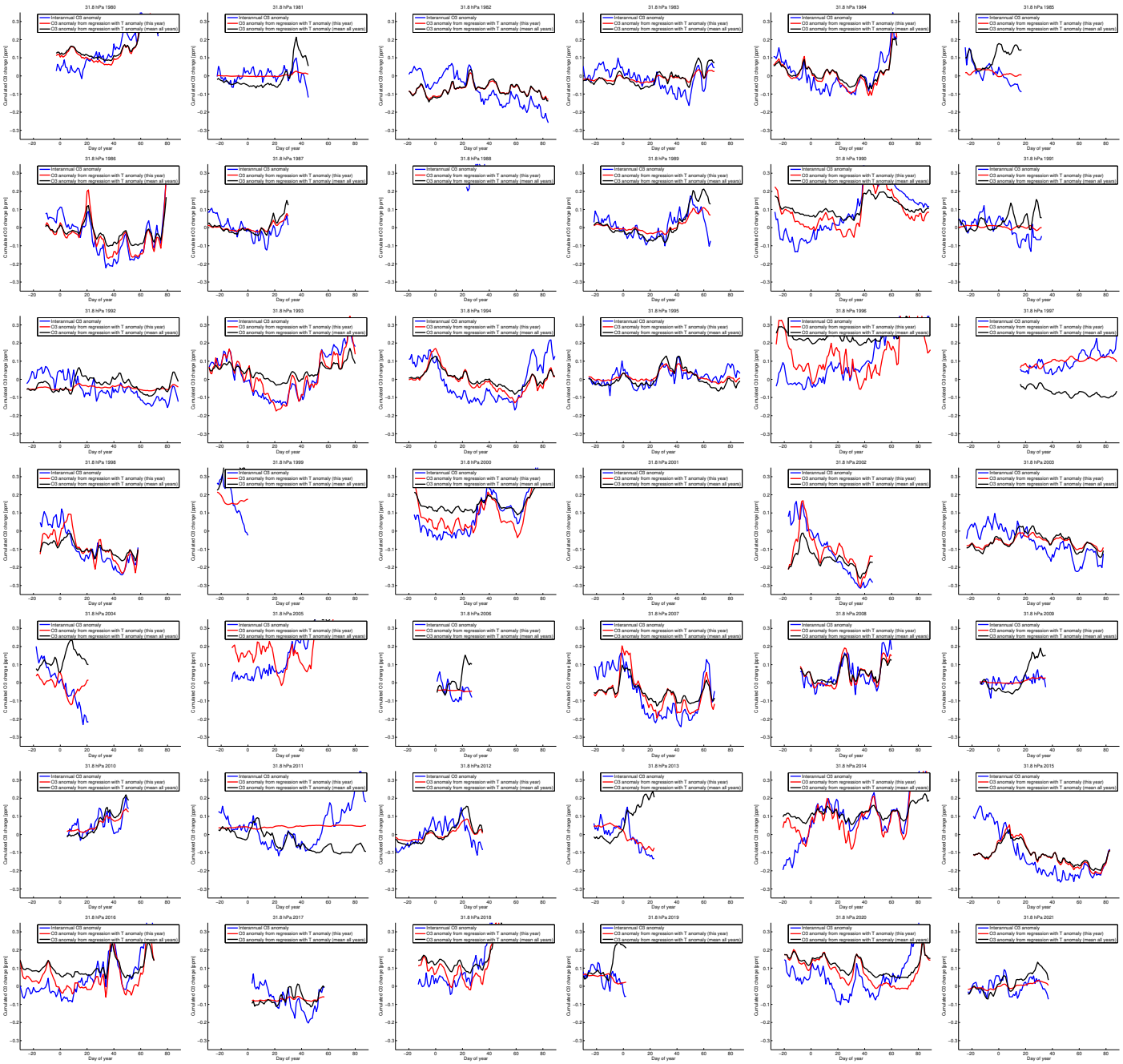

Figure S19: Anomaly of the cumulated vortex-averaged ozone change by transport at 32 hPa (layer 4) for the northern hemispheric winters 1979/1980–2020/2021 (blue, after subtraction of the change by transport that is constant in every year), vortex-averaged temperatures of the individual years regressed on the ozone anomaly (red) and vortex-averaged temperatures scaled by the mean slope of the regressions of all years (black) (cf. Figure 3 of the main manuscript).

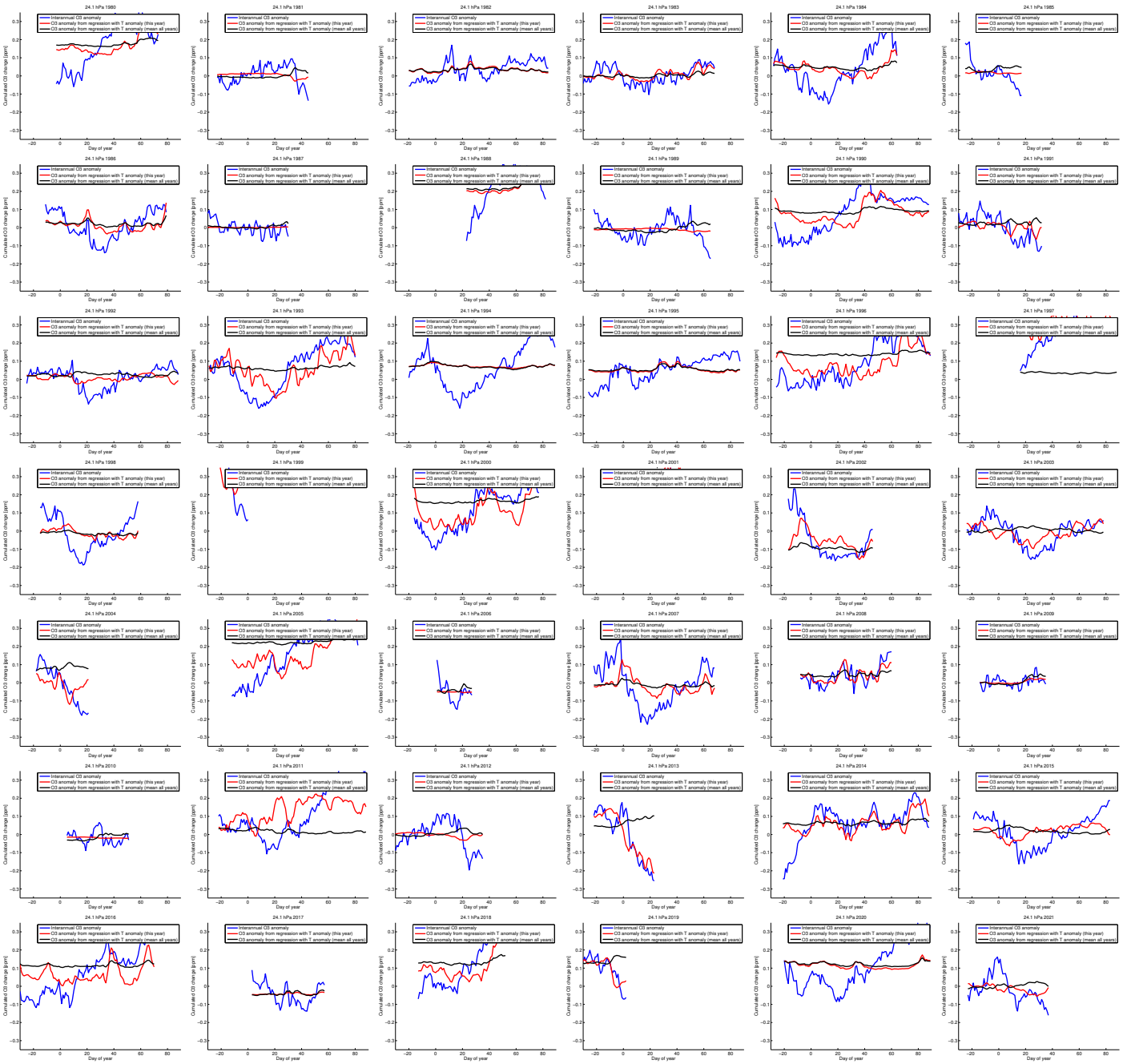

Figure S20: Anomaly of the cumulated vortex-averaged ozone change by transport at 24 hPa (layer 5) for the northern hemispheric winters 1979/1980–2020/2021 (blue, after subtraction of the change by transport that is constant in every year), vortex-averaged temperatures of the individual years regressed on the ozone anomaly (red) and vortex-averaged temperatures scaled by the mean slope of the regressions of all years (black) (cf. Figure 3 of the main manuscript).

5 Vortex mean temperatures (northern hemisphere)

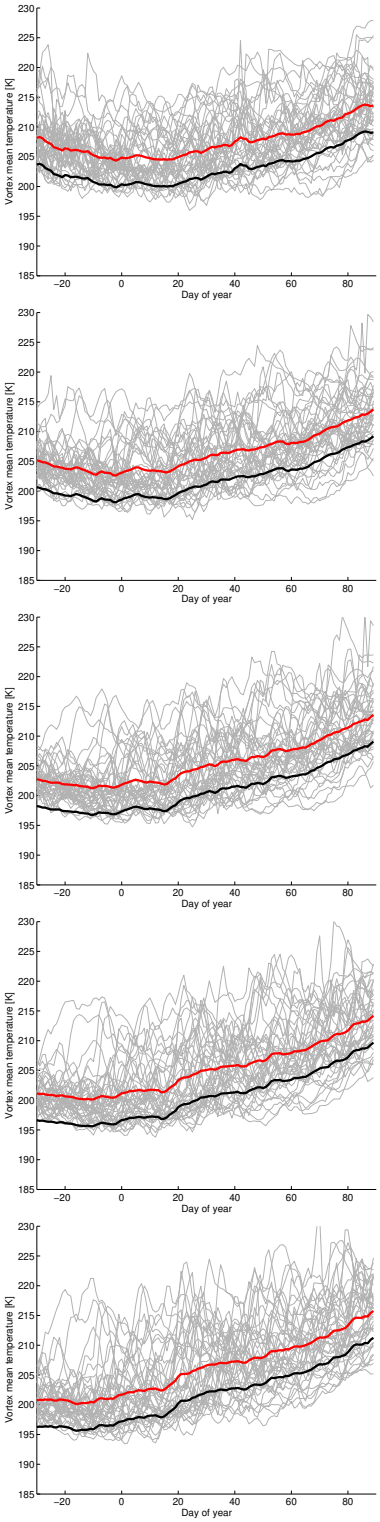

Figure S21: Vortex mean temperatures at the SWIFT levels as a function of day of year for all individual years from 1979/1980 to 2020/2021 based on ERA5 (grey lines), vortex mean temperature averaged over all years (red) and the same curve shifted by $-4.5\,\mathrm{K}$ as an approximation of the lower envelope of the grey lines (black) (cf. Figure 4 of the main manuscript).

6 Validation of the transport term (northern hemisphere)

Figure S22: Cumulated vortex-averaged ozone change by transport at 70 hPa (layer 1) for the northern hemispheric winters 1979/1980–2020/2021 (blue) and a simulation of the cumulated change by transport by a stand-alone version of the transport parameterization (red). The thin grey line shows a simulation with only the constant term, and the thin black line shows a simulation with the constant and temperature-dependent term, but without subtracting the change of the radiative equilibrium temperature from the vortex-averaged temperature change (cf. Figure 5 of the main manuscript).

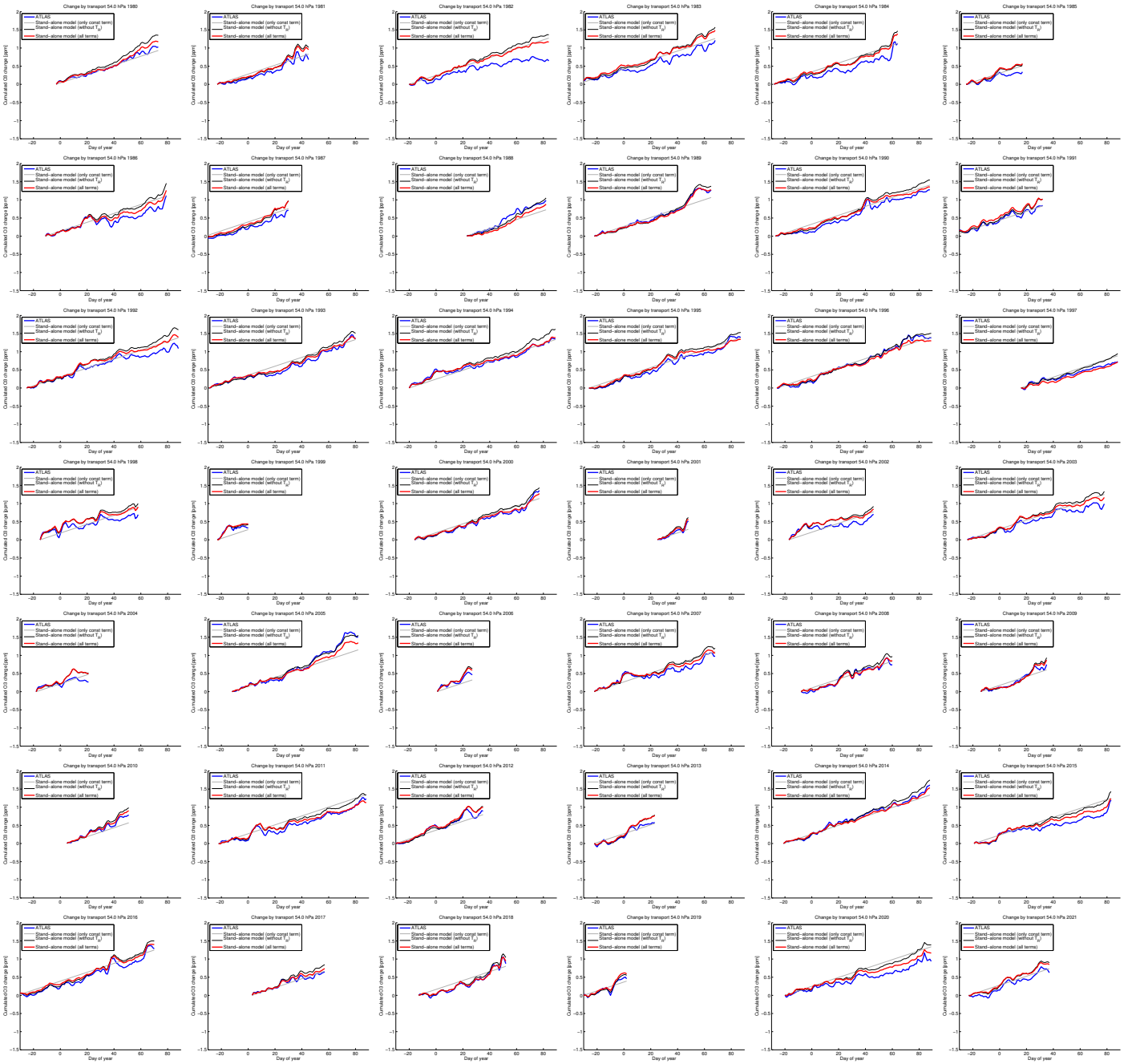

Figure S23: Cumulated vortex-averaged ozone change by transport at 54 hPa (layer 2) for the northern hemispheric winters 1979/1980–2020/2021 (blue) and a simulation of the cumulated change by transport by a stand-alone version of the transport parameterization (red). The thin grey line shows a simulation with only the constant term, and the thin black line shows a simulation with the constant and temperature-dependent term, but without subtracting the change of the radiative equilibrium temperature from the vortex-averaged temperature change (cf. Figure 5 of the main manuscript).

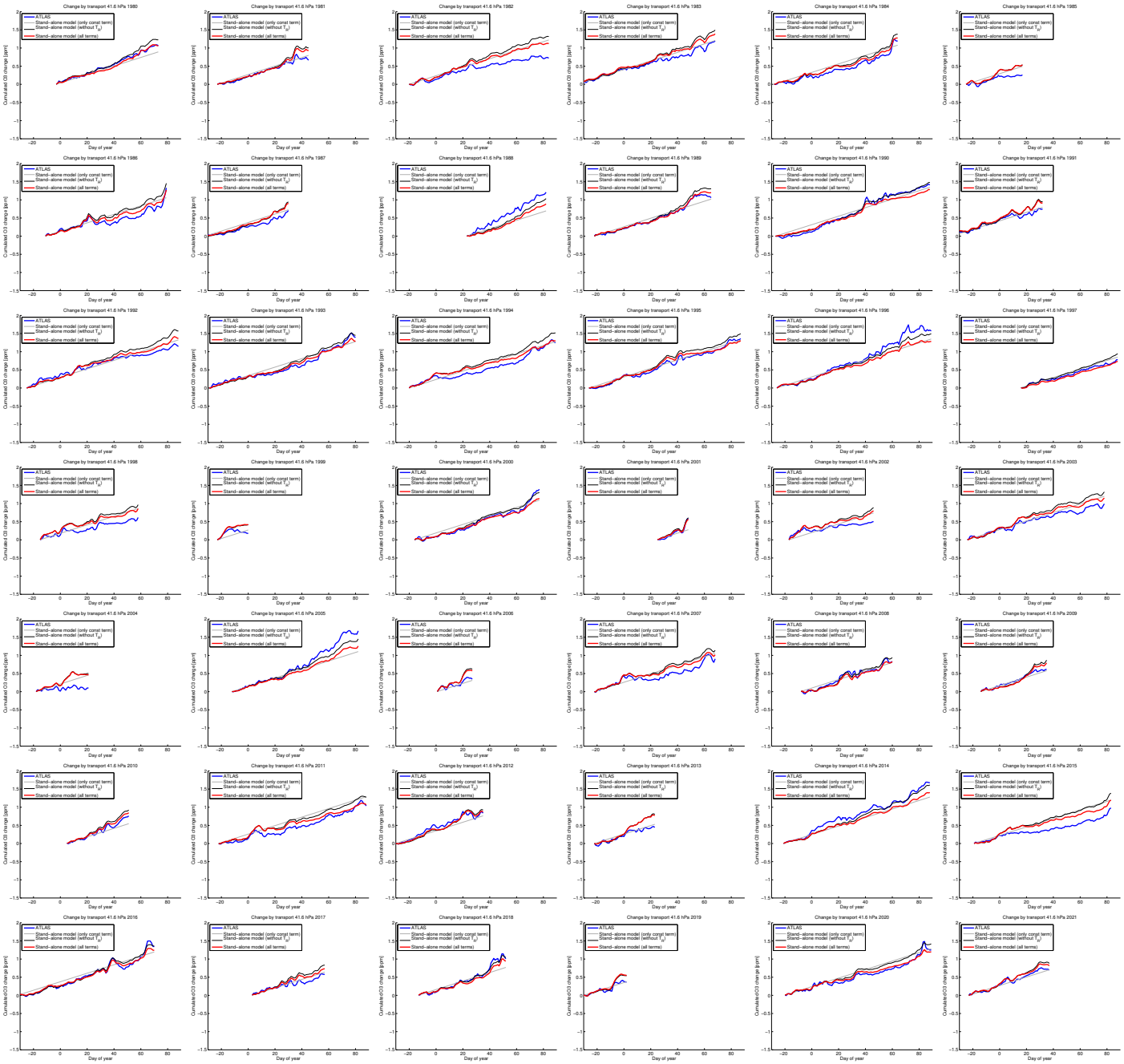

Figure S24: Cumulated vortex-averaged ozone change by transport at 42 hPa (layer 3) for the northern hemispheric winters 1979/1980–2020/2021 (blue) and a simulation of the cumulated change by transport by a stand-alone version of the transport parameterization (red). The thin grey line shows a simulation with only the constant term, and the thin black line shows a simulation with the constant and temperature-dependent term, but without subtracting the change of the radiative equilibrium temperature from the vortex-averaged temperature change (cf. Figure 5 of the main manuscript).

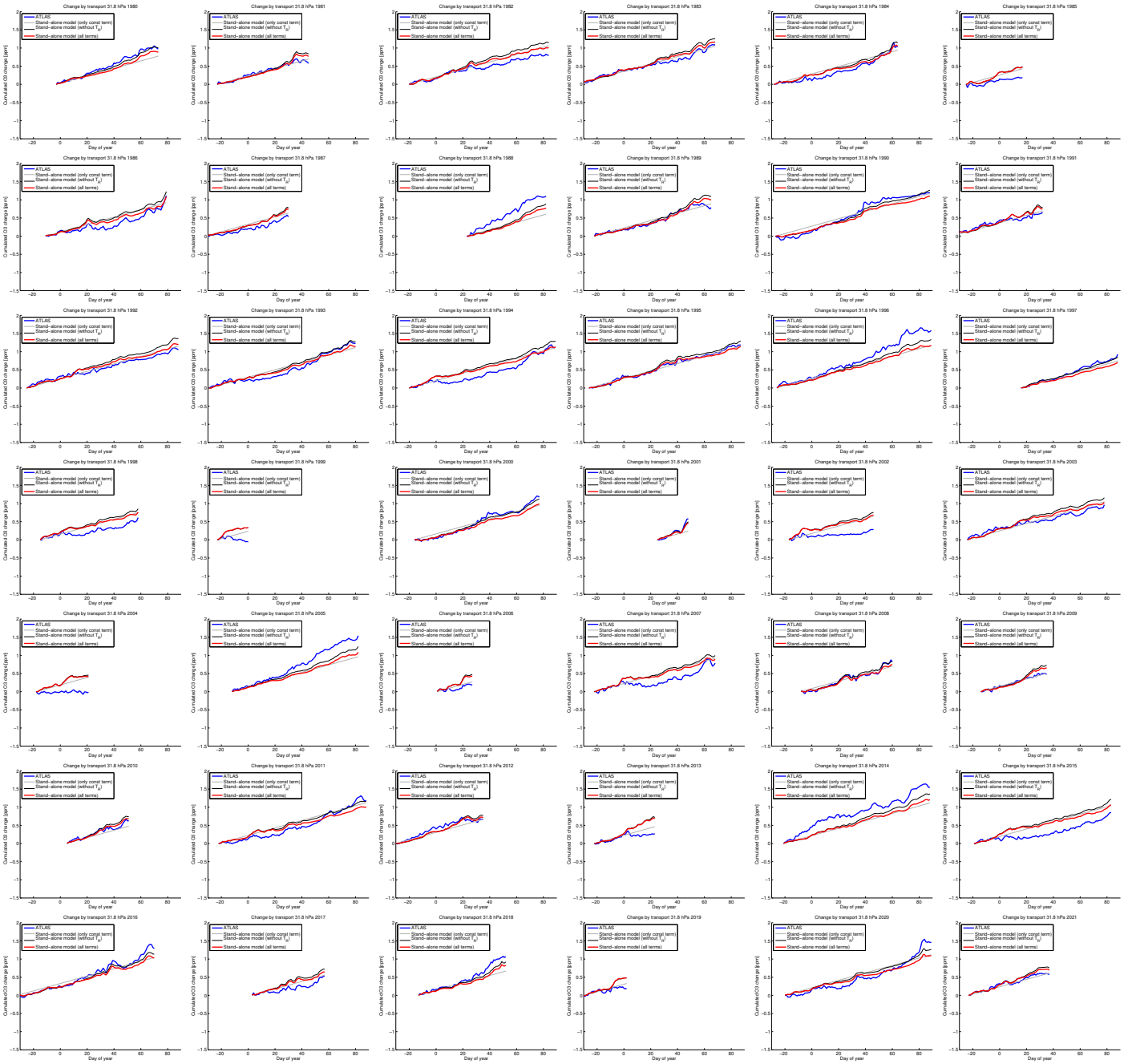

Figure S25: Cumulated vortex-averaged ozone change by transport at 32 hPa (layer 4) for the northern hemispheric winters 1979/1980–2020/2021 (blue) and a simulation of the cumulated change by transport by a stand-alone version of the transport parameterization (red). The thin grey line shows a simulation with only the constant term, and the thin black line shows a simulation with the constant and temperature-dependent term, but without subtracting the change of the radiative equilibrium temperature from the vortex-averaged temperature change (cf. Figure 5 of the main manuscript).

Figure S26: Cumulated vortex-averaged ozone change by transport at 24 hPa (layer 5) for the northern hemispheric winters 1979/1980–2020/2021 (blue) and a simulation of the cumulated change by transport by a stand-alone version of the transport parameterization (red). The thin grey line shows a simulation with only the constant term, and the thin black line shows a simulation with the constant and temperature-dependent term, but without subtracting the change of the radiative equilibrium temperature from the vortex-averaged temperature change (cf. Figure 5 of the main manuscript).

7 Validation of the complete SWIFT model (northern hemisphere)

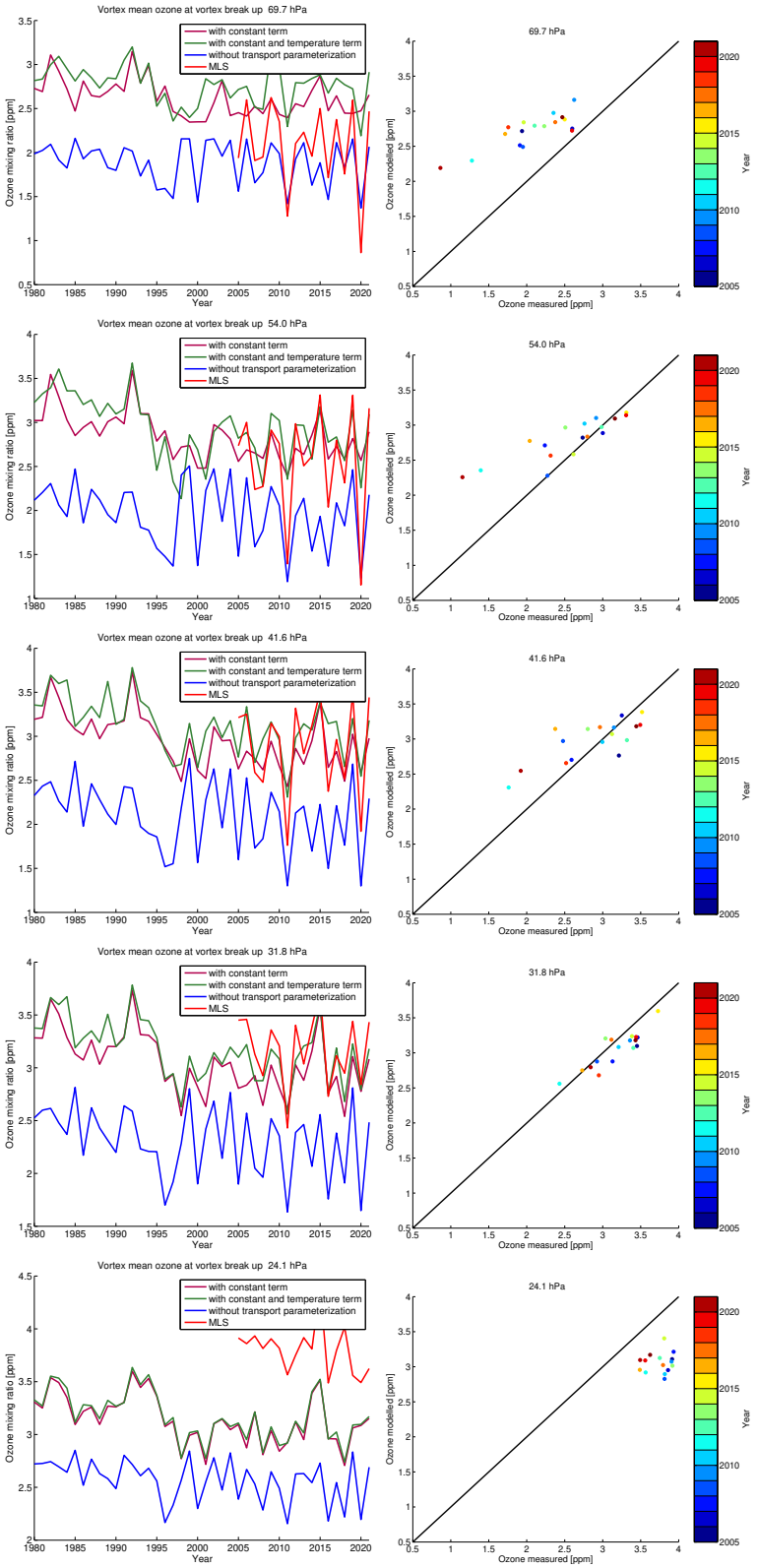

Figure S27: Left (cf. Figure 6 of the main manuscript): Vortex-averaged ozone simulated by the stand-alone Polar SWIFT model for the date of vortex breakup in the northern hemisphere for different years. Ozone mixing ratios simulated without the transport parameterization (blue), ozone mixing ratios simulated with only the "constant change" term of the transport parameterization (brown), ozone mixing ratios simulated with the full transport parameterization with the "constant change" term and temperature-dependent term (green), and corresponding measurements of ozone from the MLS instrument (red). Right (cf. Figure 7 of the main manuscript): Scatter plot of the same data.

8 Difference transport term at vortex breakup of transport parameterization to ATLAS (northern hemisphere)

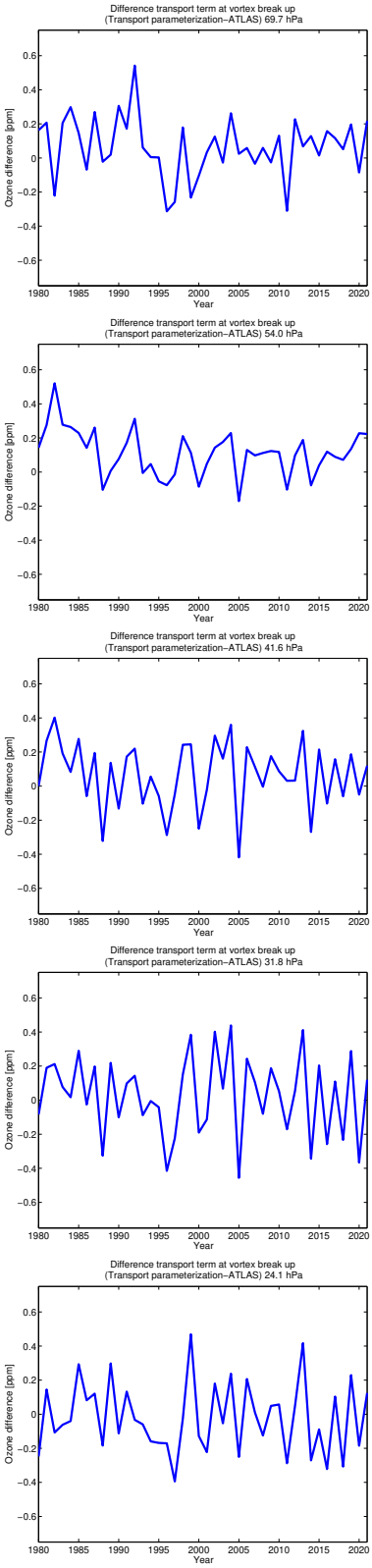

Figure S28: Difference of cumulated vortex-averaged ozone change by transport at vortex break up between the transport parameterization and ATLAS-SWIFT for the northern hemispheric winters 1979/1980–2020/2021.

9 Observed change (southern hemisphere)

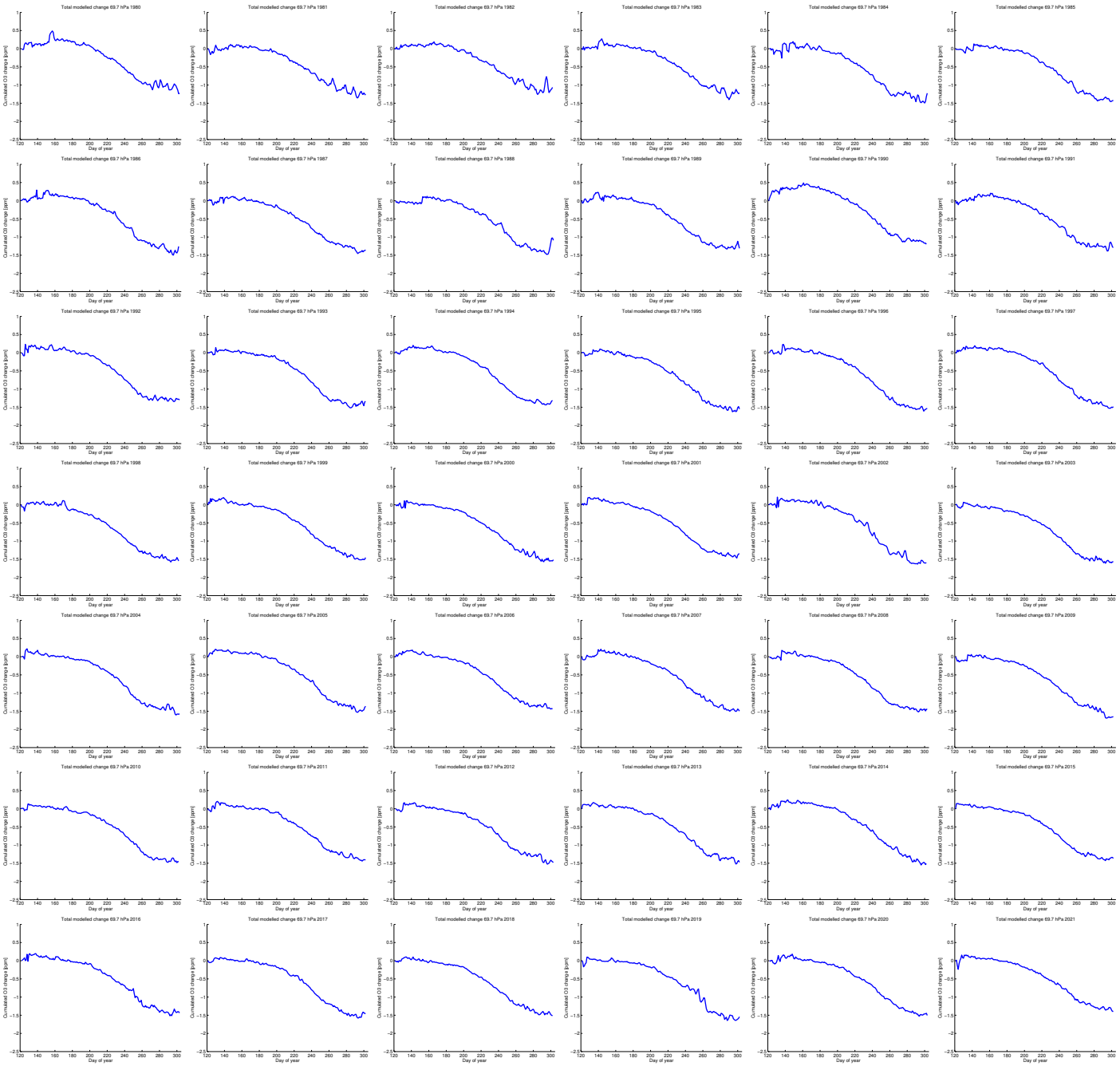

Figure S29: Cumulated total change of vortex-averaged ozone mixing ratio for the southern hemispheric winters 1980–2021 at 70 hPa (layer 1) simulated by ATLAS-SWIFT as a function of the day of year (cf. Figure 1 of the main manuscript).

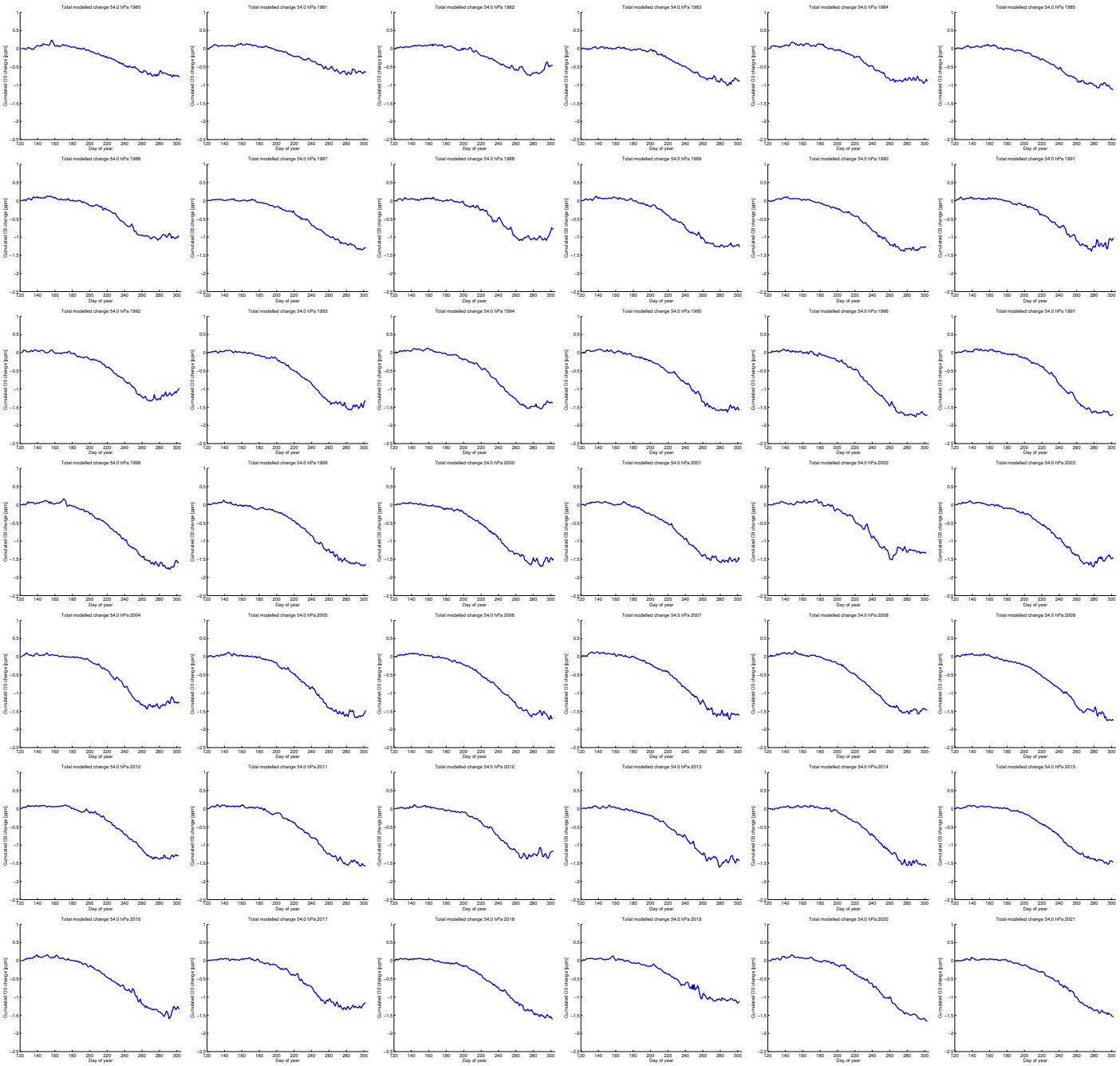

Figure S30: Cumulated total change of vortex-averaged ozone mixing ratio for the southern hemispheric winters 1980–2021 at 54 hPa (layer 2) simulated by ATLAS-SWIFT as a function of the day of year (cf. Figure 1 of the main manuscript).

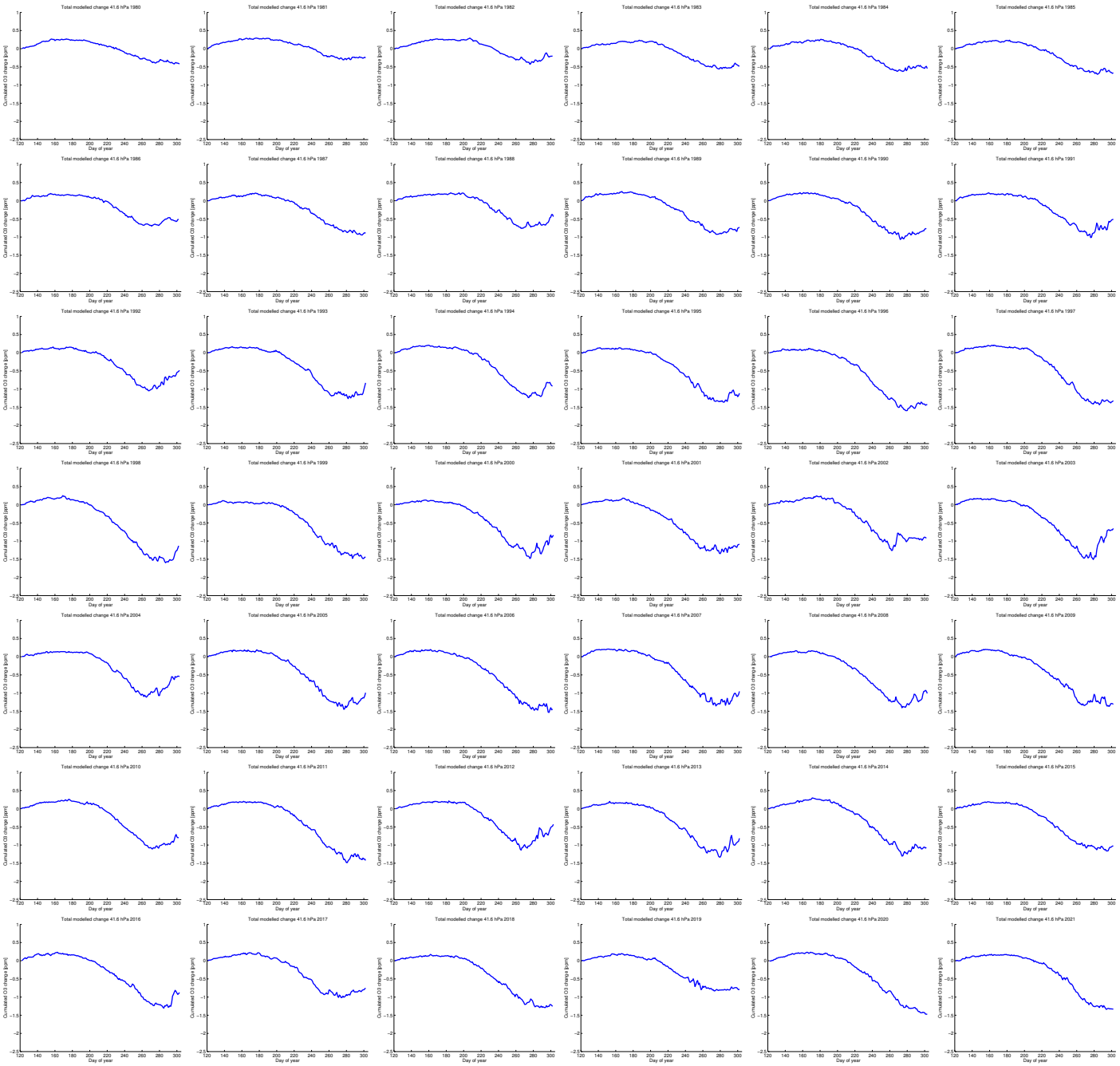

Figure S31: Cumulated total change of vortex-averaged ozone mixing ratio for the southern hemispheric winters 1980–2021 at 42 hPa (layer 3) simulated by ATLAS-SWIFT as a function of the day of year (cf. Figure 1 of the main manuscript).

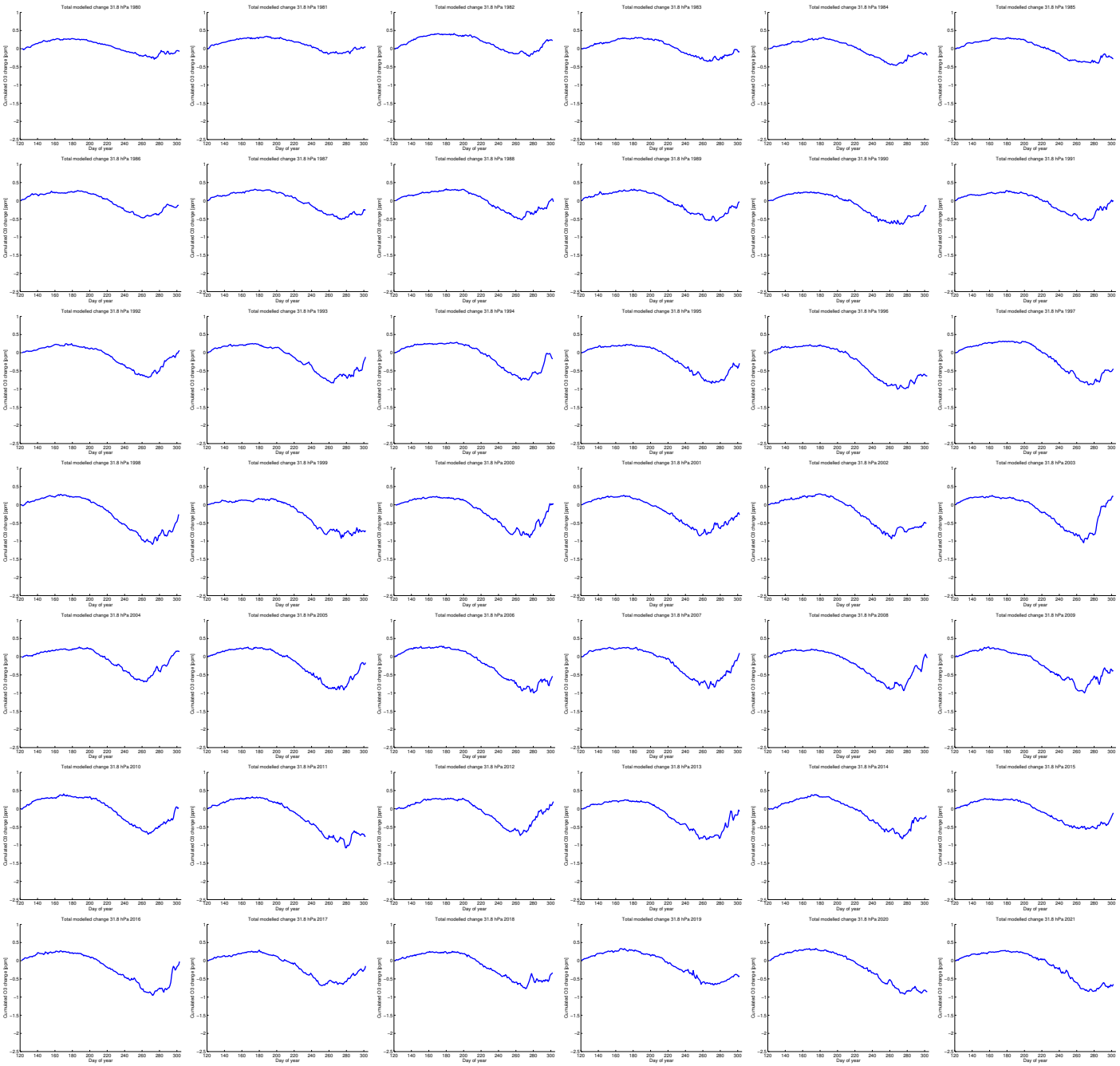

Figure S32: Cumulated total change of vortex-averaged ozone mixing ratio for the southern hemispheric winters 1980–2021 at 32 hPa (layer 4) simulated by ATLAS-SWIFT as a function of the day of year (cf. Figure 1 of the main manuscript).

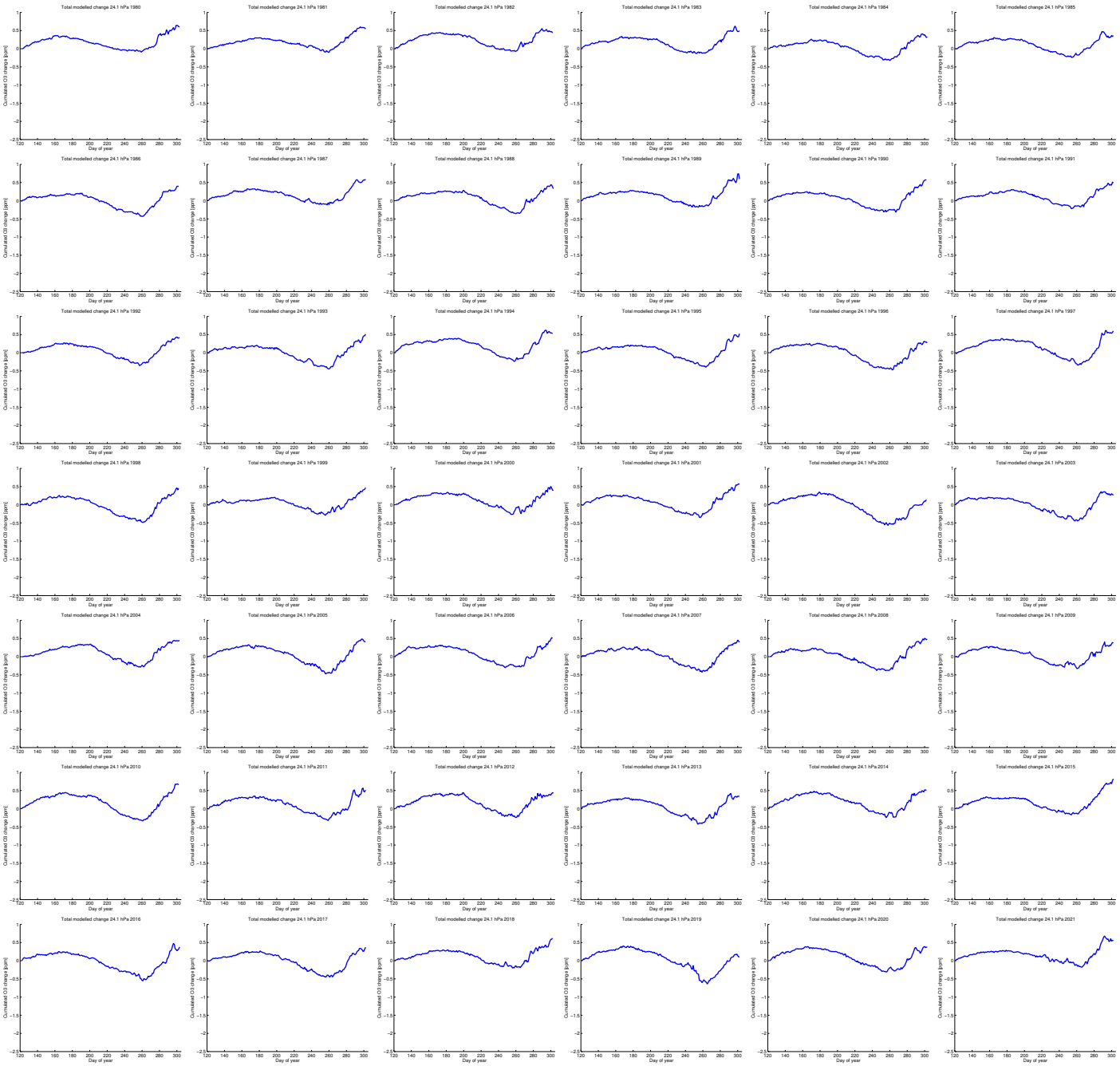

Figure S33: Cumulated total change of vortex-averaged ozone mixing ratio for the southern hemispheric winters 1980–2021 at 24 hPa (layer 5) simulated by ATLAS-SWIFT as a function of the day of year (cf. Figure 1 of the main manuscript).

10 Chemical change (southern hemisphere)

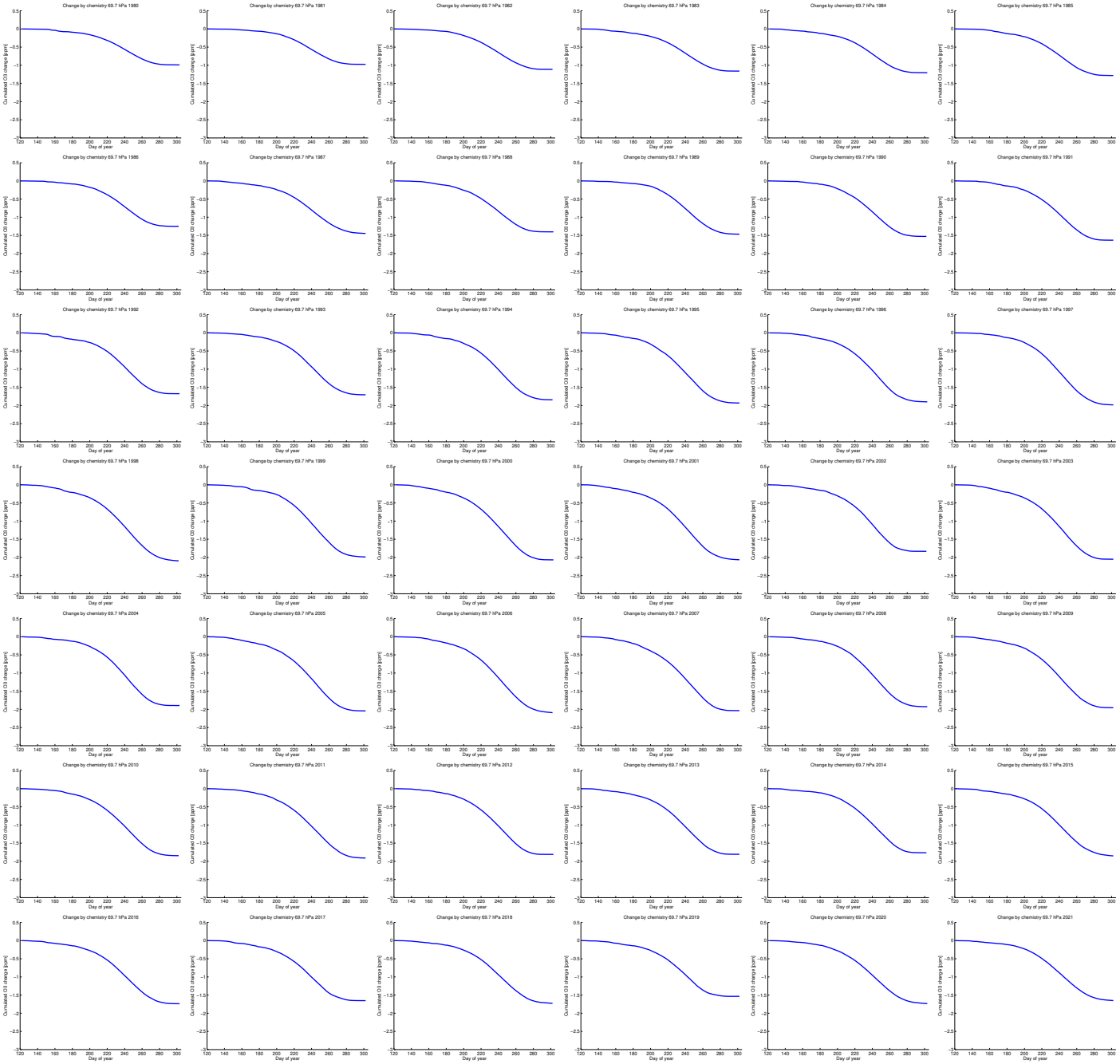

Figure S34: Cumulated change by chemistry of vortex-averaged ozone mixing ratio for the southern hemispheric winters 1980–2021 at 70 hPa (layer 1) simulated by ATLAS-SWIFT as a function of the day of year (cf. Figure 1 of the main manuscript).

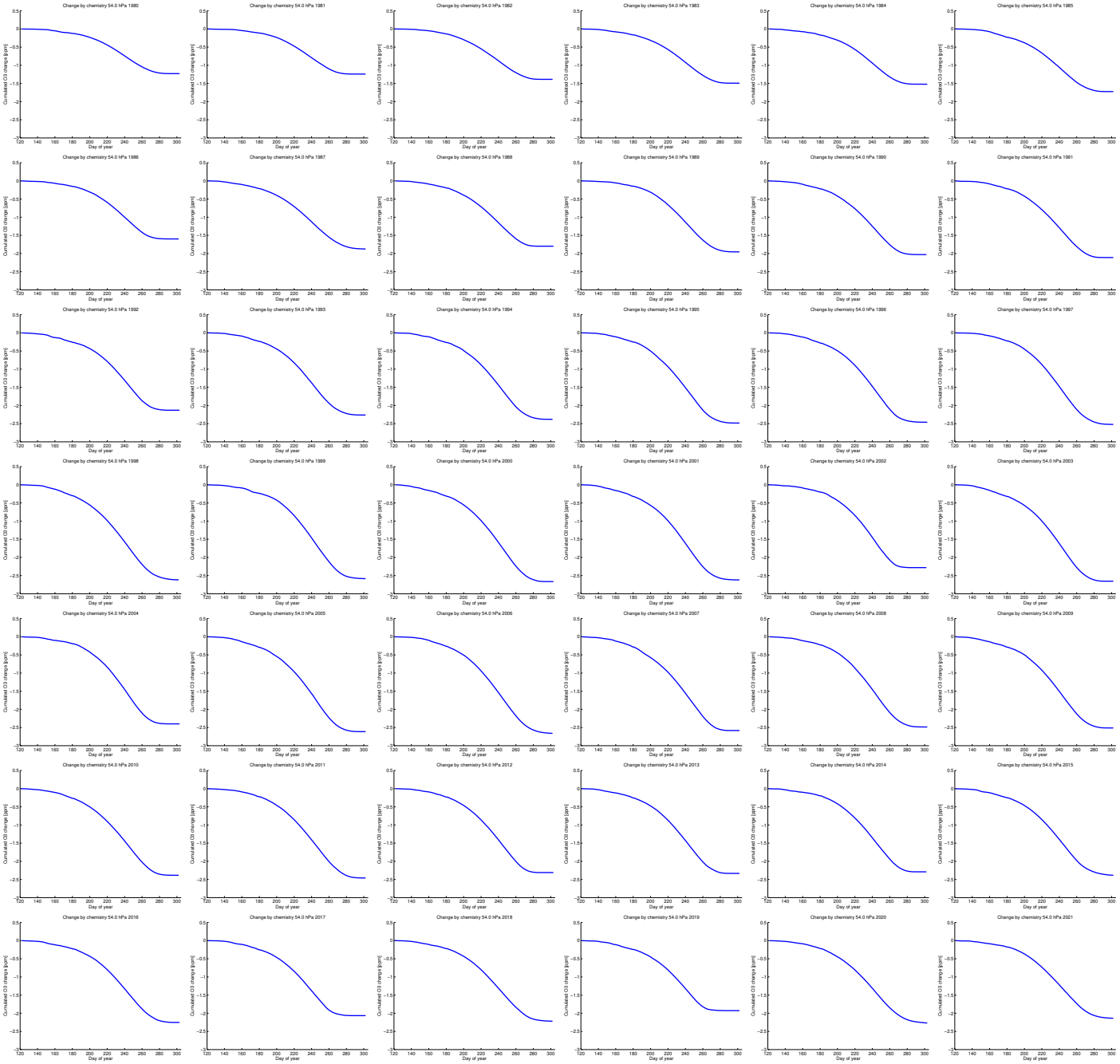

Figure S35: Cumulated change by chemistry of vortex-averaged ozone mixing ratio for the southern hemispheric winters 1980–2021 at 54 hPa (layer 2) simulated by ATLAS-SWIFT as a function of the day of year (cf. Figure 1 of the main manuscript).

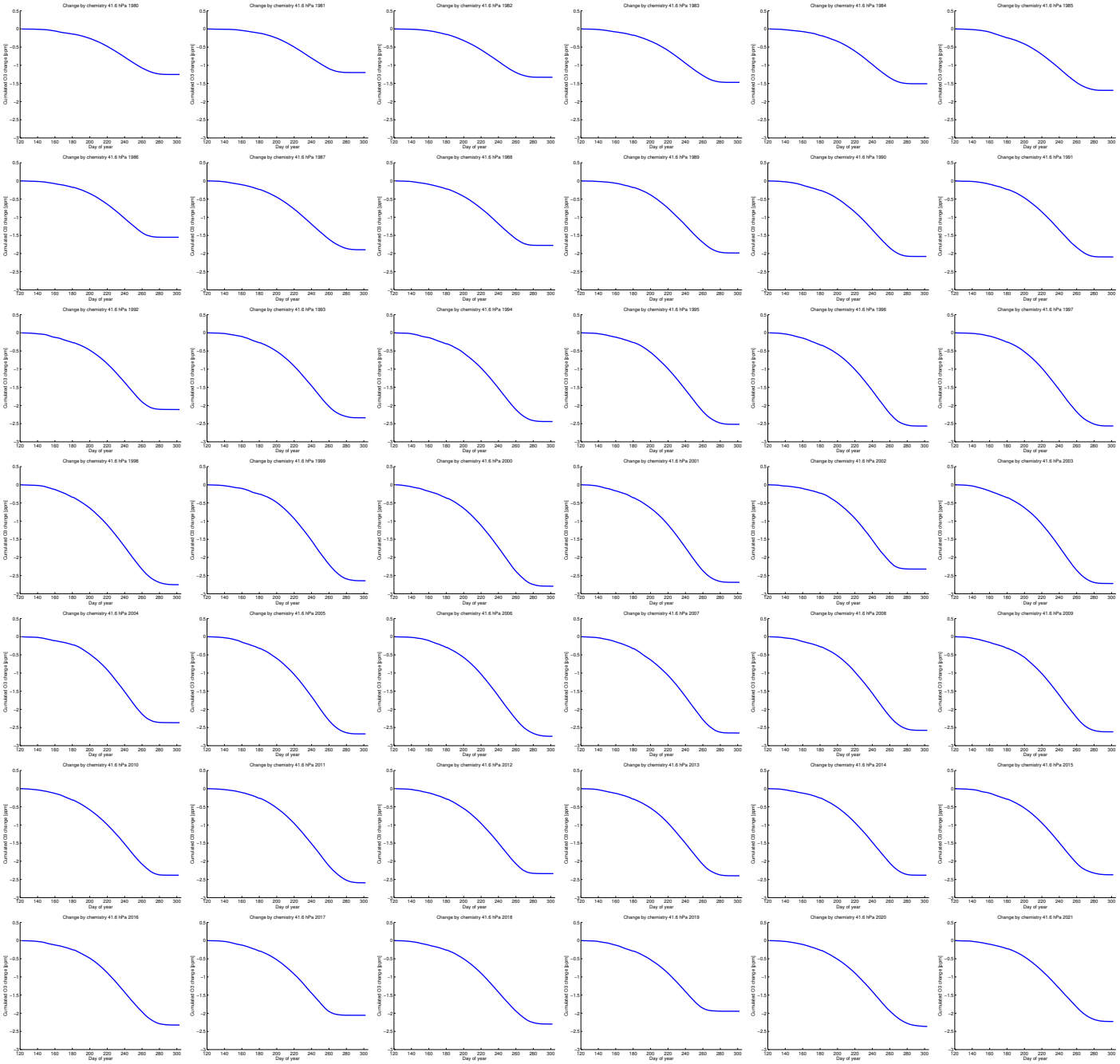

Figure S36: Cumulated change by chemistry of vortex-averaged ozone mixing ratio for the southern hemispheric winters 1980–2021 at 42 hPa (layer 3) simulated by ATLAS-SWIFT as a function of the day of year (cf. Figure 1 of the main manuscript).

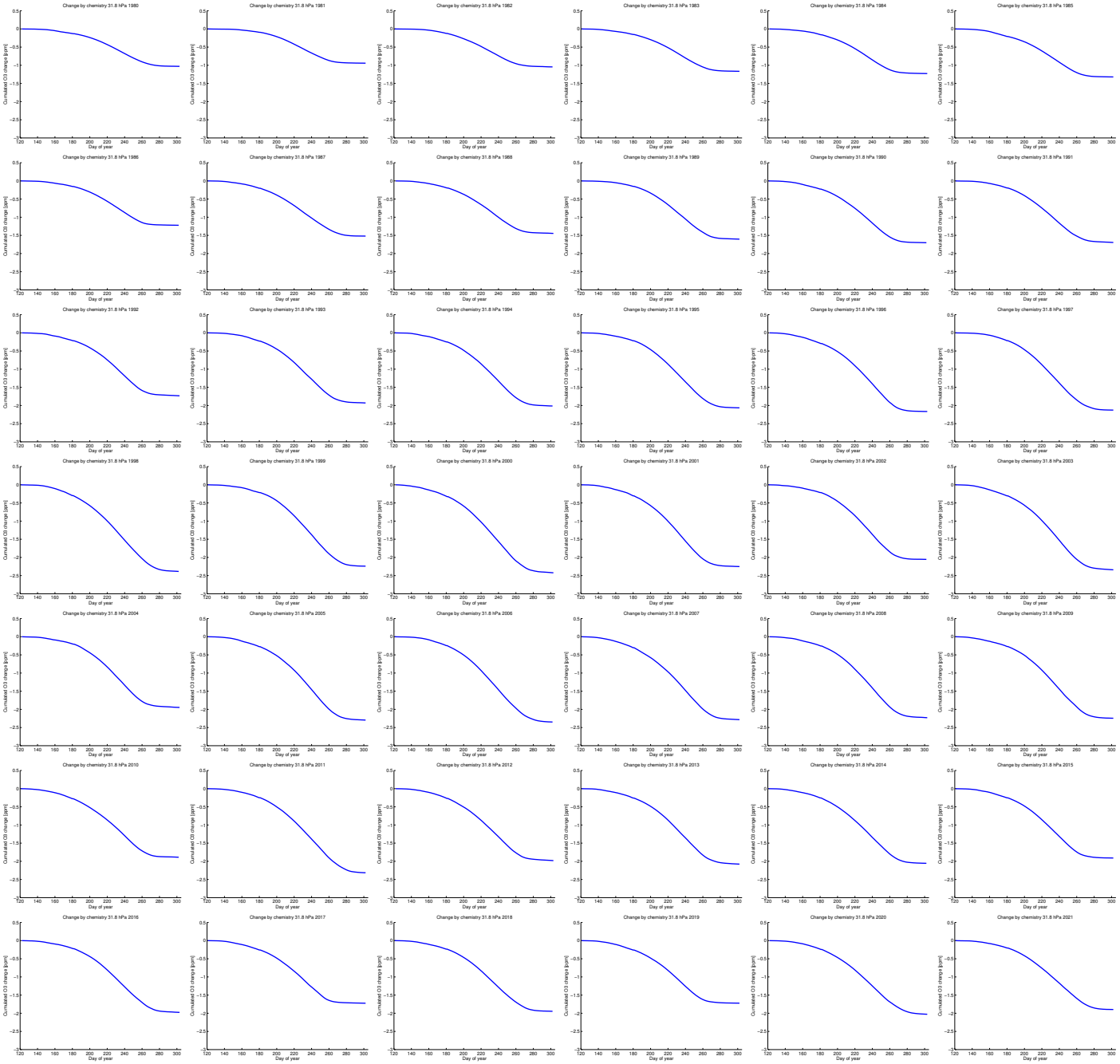

Figure S37: Cumulated change by chemistry of vortex-averaged ozone mixing ratio for the southern hemispheric winters 1980–2021 at 32 hPa (layer 4) simulated by ATLAS-SWIFT as a function of the day of year (cf. Figure 1 of the main manuscript).

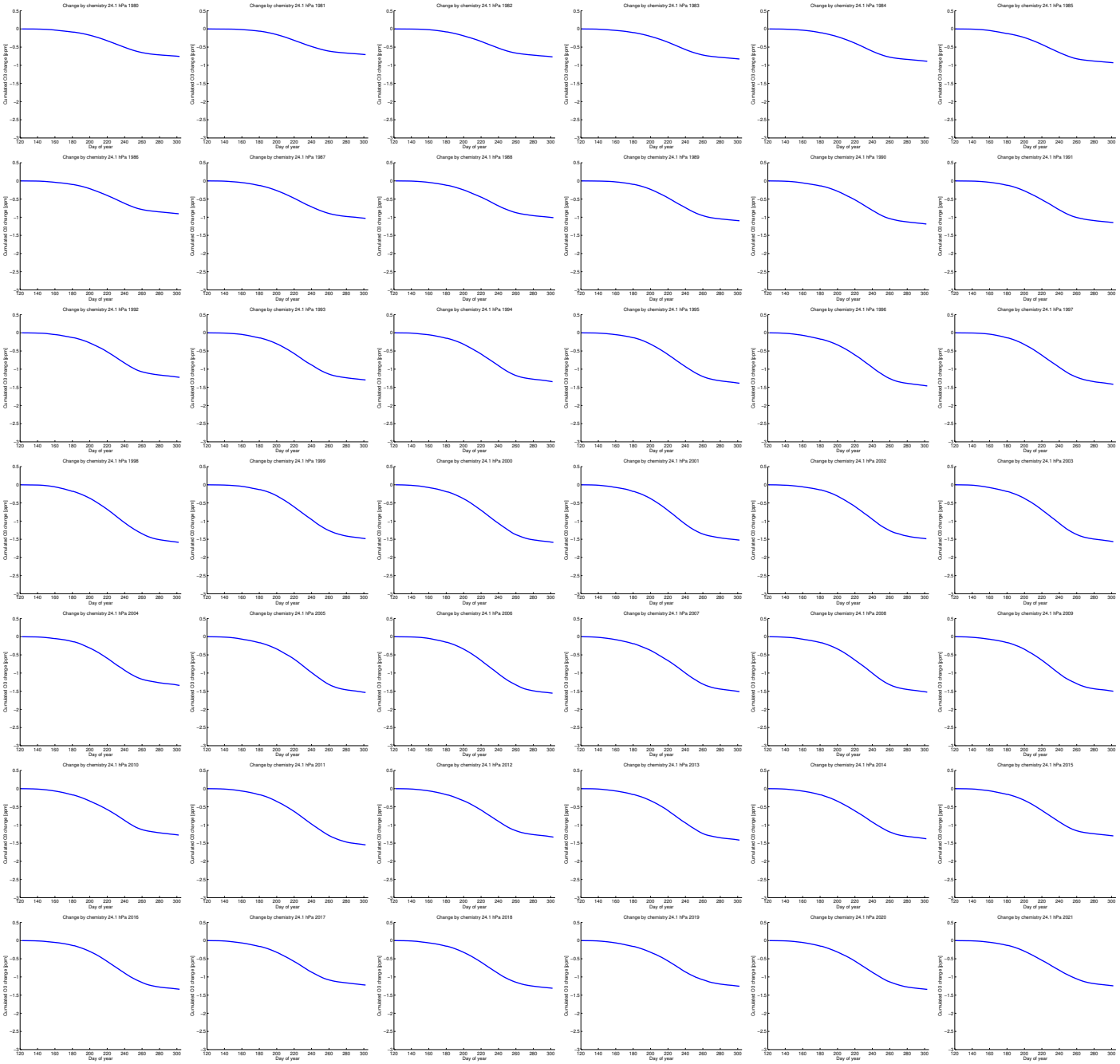

Figure S38: Cumulated change by chemistry of vortex-averaged ozone mixing ratio for the southern hemispheric winters 1980–2021 at 24 hPa (layer 5) simulated by ATLAS-SWIFT as a function of the day of year (cf. Figure 1 of the main manuscript).

11 Transport change and fit for constant term (southern hemisphere)

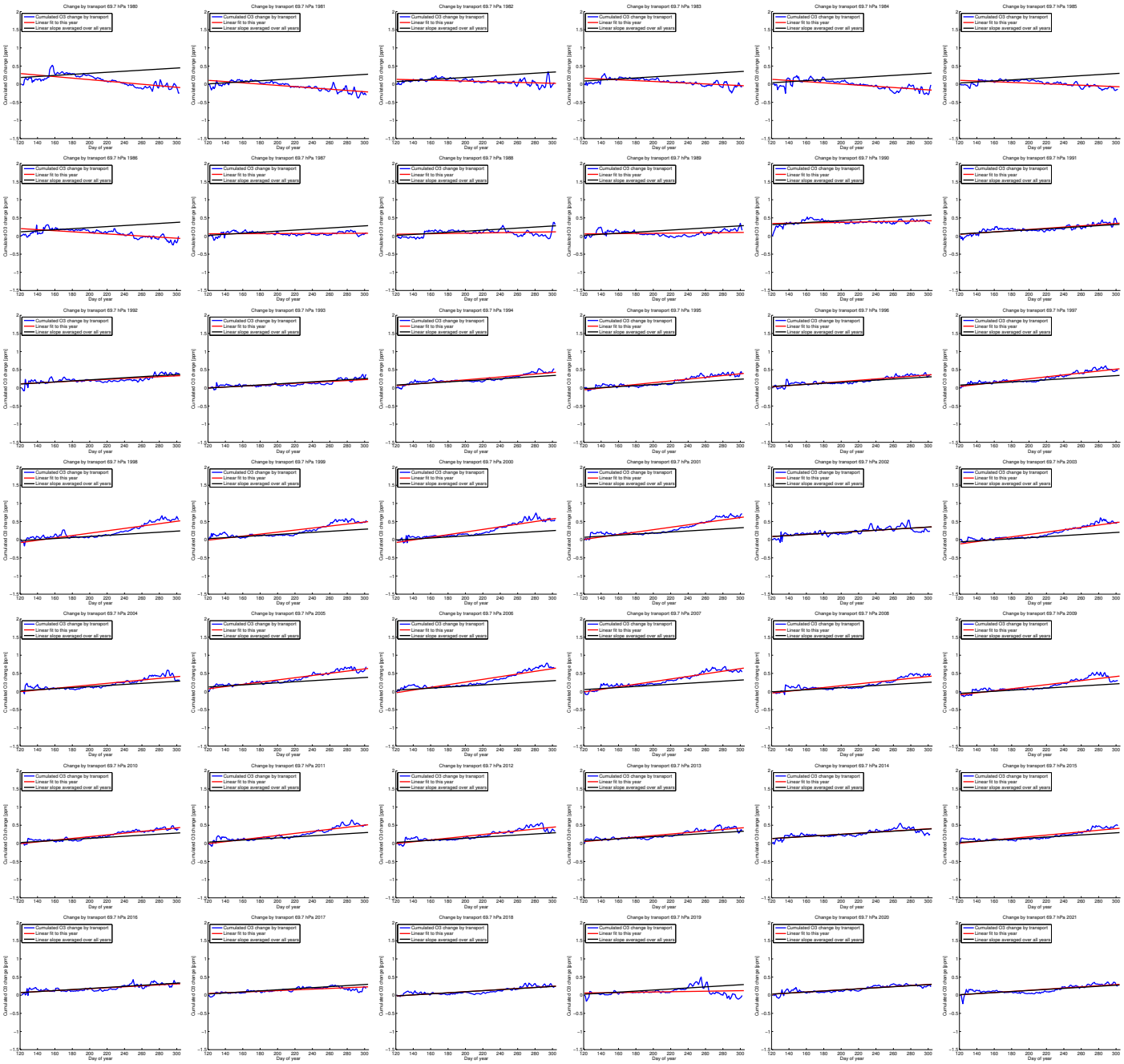

Figure S39: Cumulated change by transport of vortex-averaged ozone mixing ratio for the southern hemispheric winters 1980–2021 at 70 hPa (layer 1) simulated by ATLAS-SWIFT as a function of the day of year (blue), linear fit to the cumulated change (red) and linear slope based on the averaged slope of the fits of all years (black) (cf. Figure 1 and 2 of the main manuscript).

Figure S40: Cumulated change by transport of vortex-averaged ozone mixing ratio for the southern hemispheric winters 1980–2021 at 54 hPa (layer 2) simulated by ATLAS-SWIFT as a function of the day of year (blue), linear fit to the cumulated change (red) and linear slope based on the averaged slope of the fits of all years (black) (cf. Figure 1 and 2 of the main manuscript).

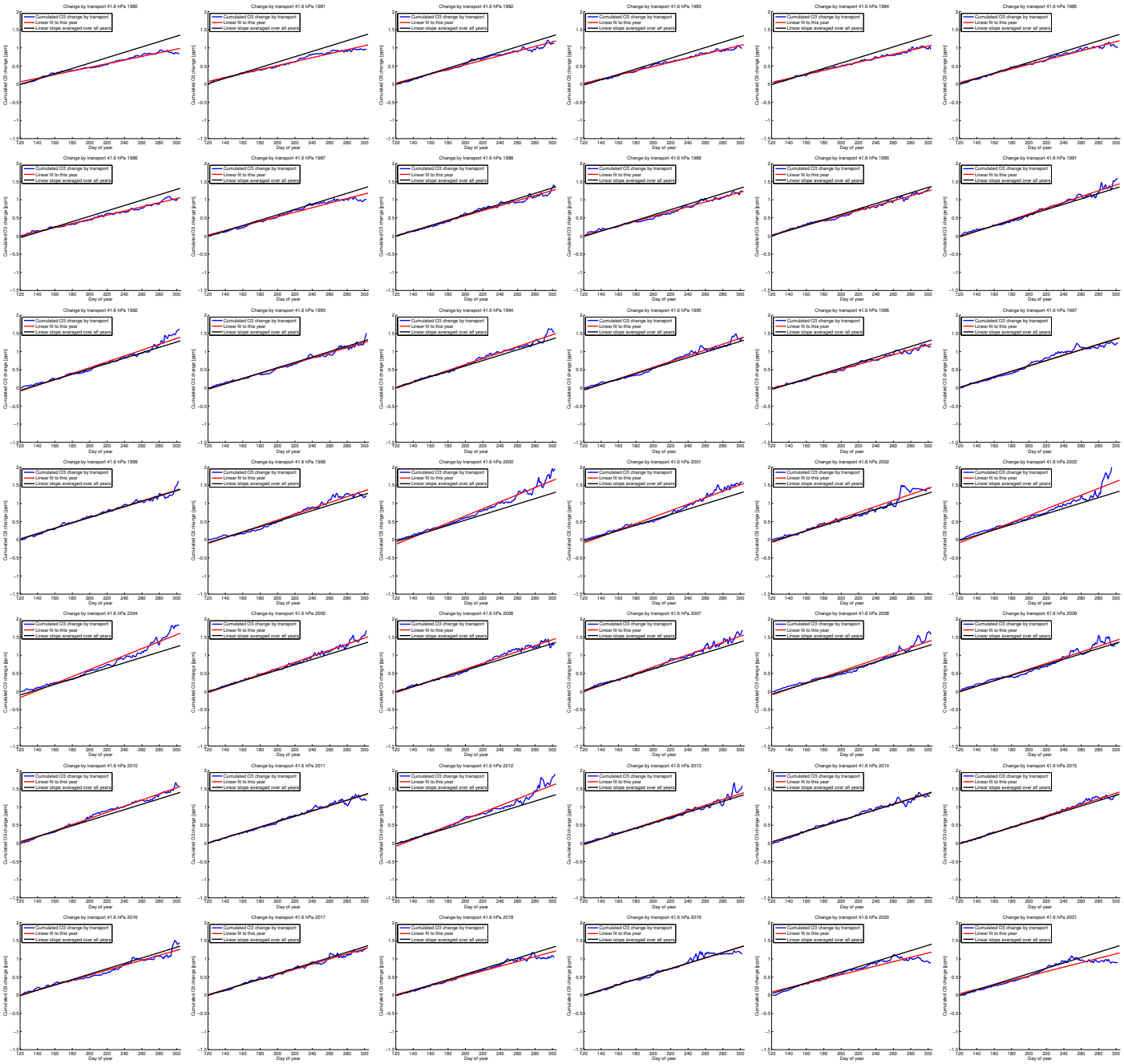

Figure S41: Cumulated change by transport of vortex-averaged ozone mixing ratio for the southern hemispheric winters 1980–2021 at 42 hPa (layer 3) simulated by ATLAS-SWIFT as a function of the day of year (blue), linear fit to the cumulated change (red) and linear slope based on the averaged slope of the fits of all years (black) (cf. Figure 1 and 2 of the main manuscript).

Figure S42: Cumulated change by transport of vortex-averaged ozone mixing ratio for the southern hemispheric winters 1980–2021 at 32 hPa (layer 4) simulated by ATLAS-SWIFT as a function of the day of year (blue), linear fit to the cumulated change (red) and linear slope based on the averaged slope of the fits of all years (black) (cf. Figure 1 and 2 of the main manuscript).

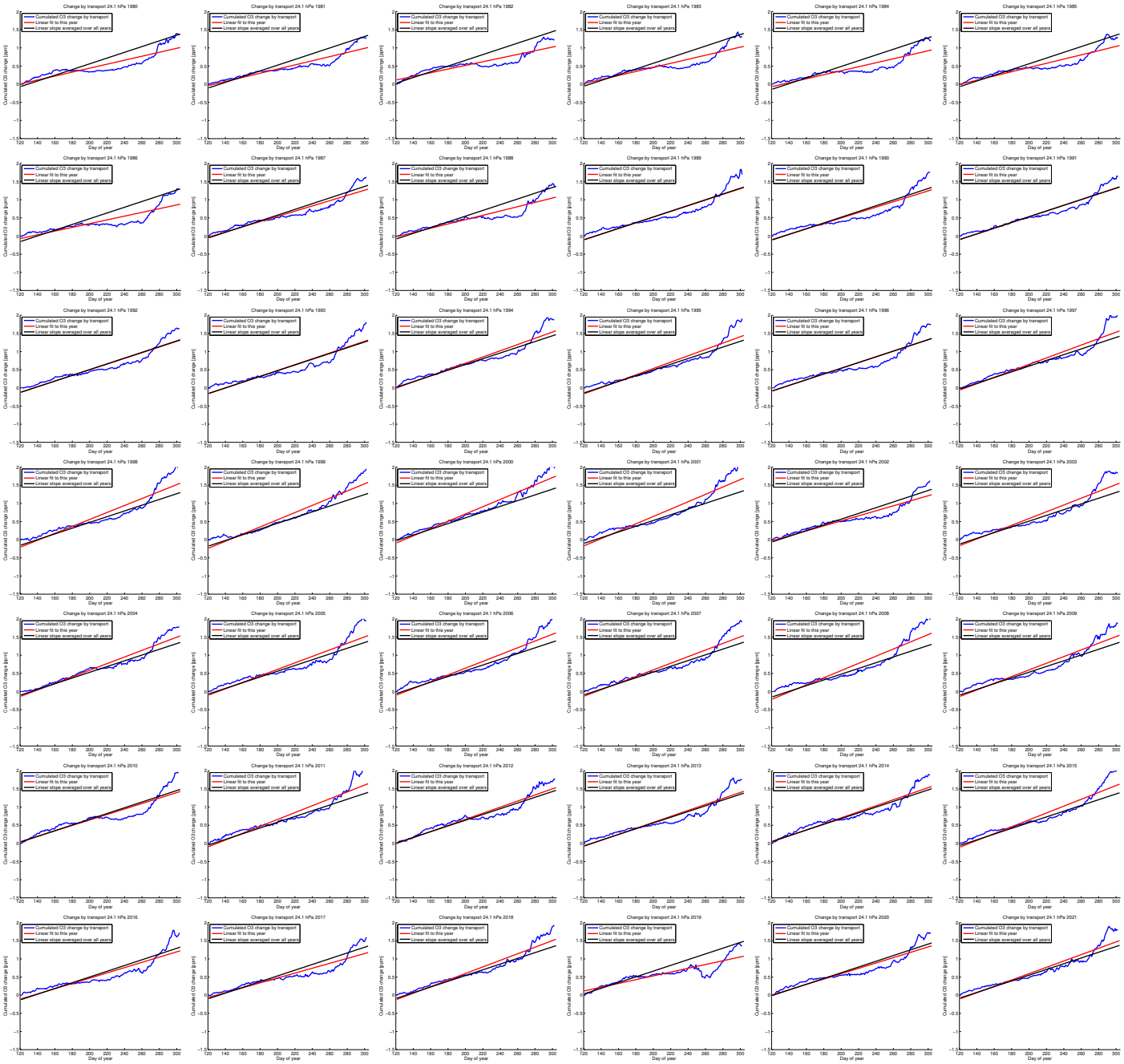

Figure S43: Cumulated change by transport of vortex-averaged ozone mixing ratio for the southern hemispheric winters 1980–2021 at 24 hPa (layer 5) simulated by ATLAS-SWIFT as a function of the day of year (blue), linear fit to the cumulated change (red) and linear slope based on the averaged slope of the fits of all years (black) (cf. Figure 1 and 2 of the main manuscript).

12 Fit for temperature-dependent term (southern hemisphere)

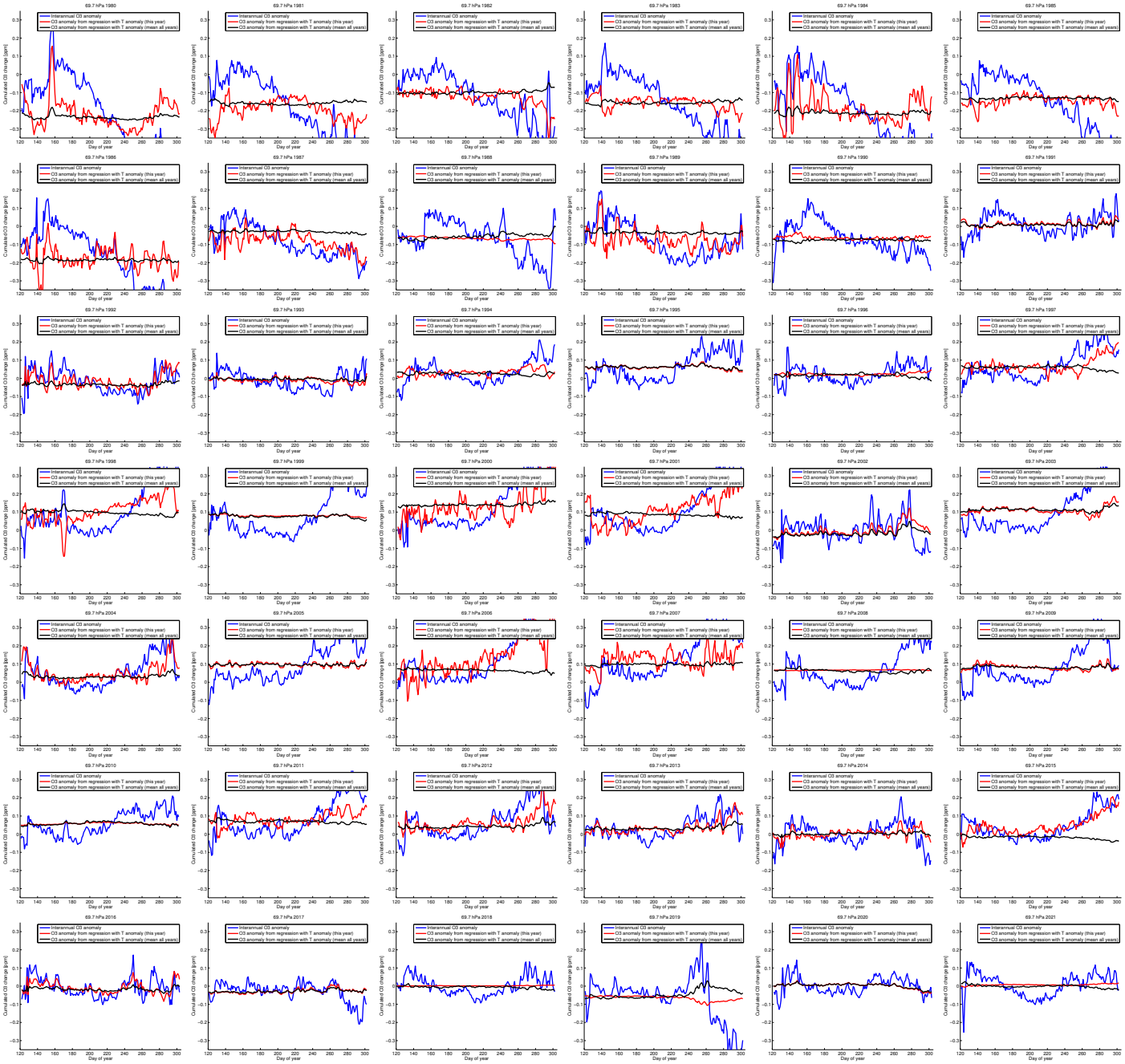

Figure S44: Anomaly of the cumulated vortex-averaged ozone change by transport at 70 hPa (layer 1) for the southern hemispheric winters 1980–2021 (blue, after subtraction of the change by transport that is constant in every year), vortex-averaged temperatures of the individual years regressed on the ozone anomaly (red) and vortex-averaged temperatures scaled by the mean slope of the regressions of all years (black) (cf. Figure 3 of the main manuscript).

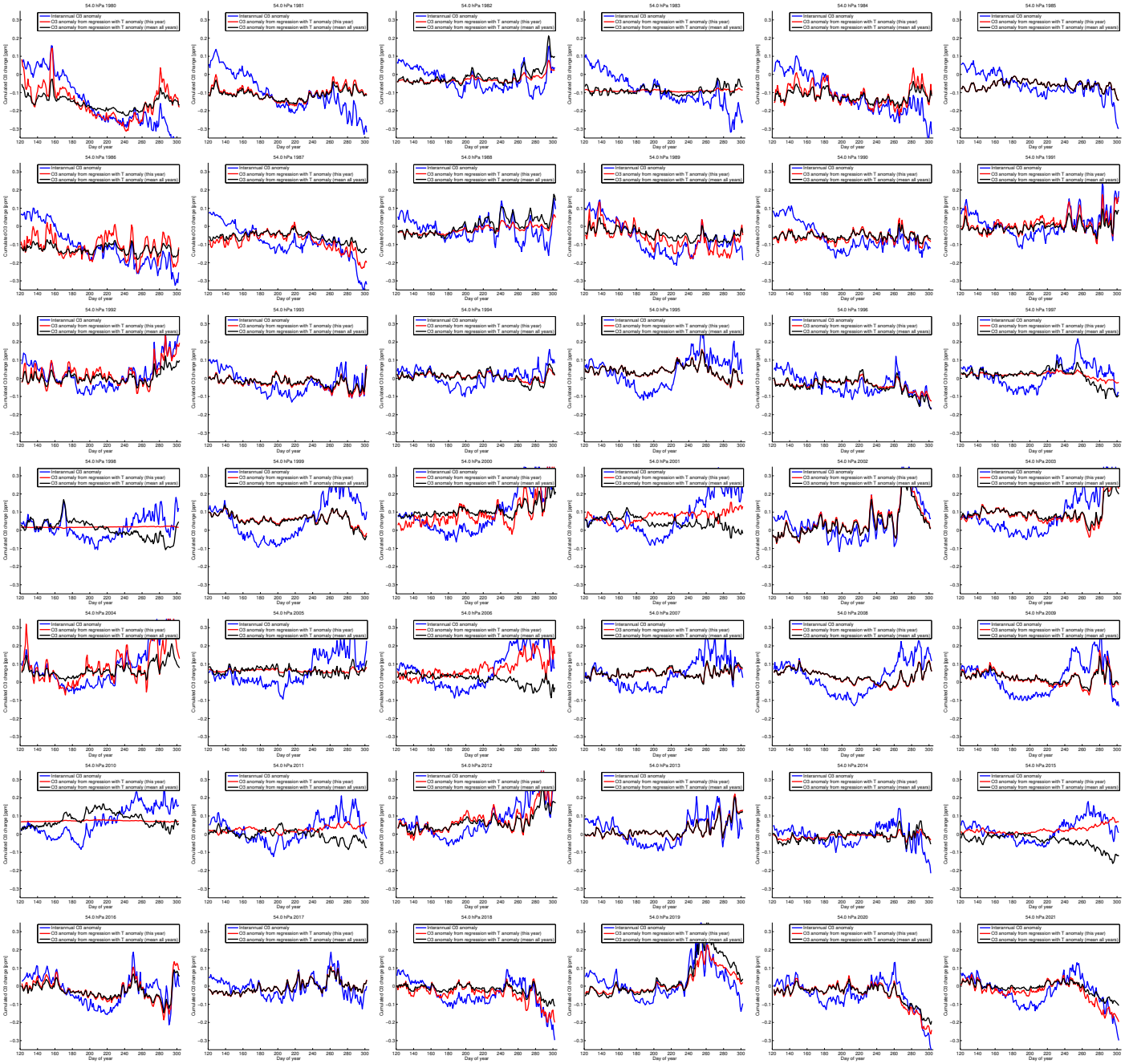

Figure S45: Anomaly of the cumulated vortex-averaged ozone change by transport at 54 hPa (layer 2) for the southern hemispheric winters 1980–2021 (blue, after subtraction of the change by transport that is constant in every year), vortex-averaged temperatures of the individual years regressed on the ozone anomaly (red) and vortex-averaged temperatures scaled by the mean slope of the regressions of all years (black) (cf. Figure 3 of the main manuscript).

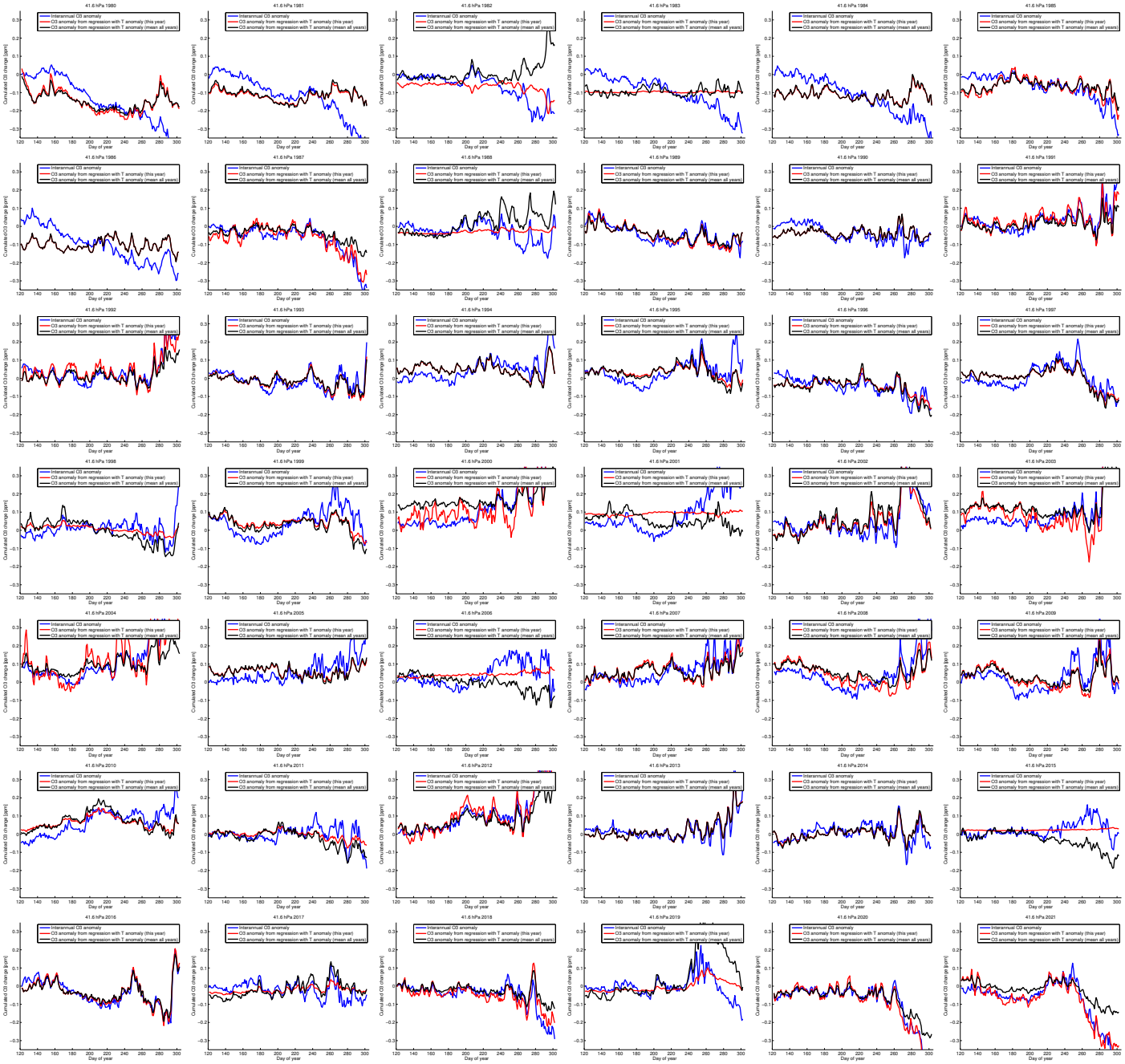

Figure S46: Anomaly of the cumulated vortex-averaged ozone change by transport at 42 hPa (layer 3) for the southern hemispheric winters 1980–2021 (blue, after subtraction of the change by transport that is constant in every year), vortex-averaged temperatures of the individual years regressed on the ozone anomaly (red) and vortex-averaged temperatures scaled by the mean slope of the regressions of all years (black) (cf. Figure 3 of the main manuscript).

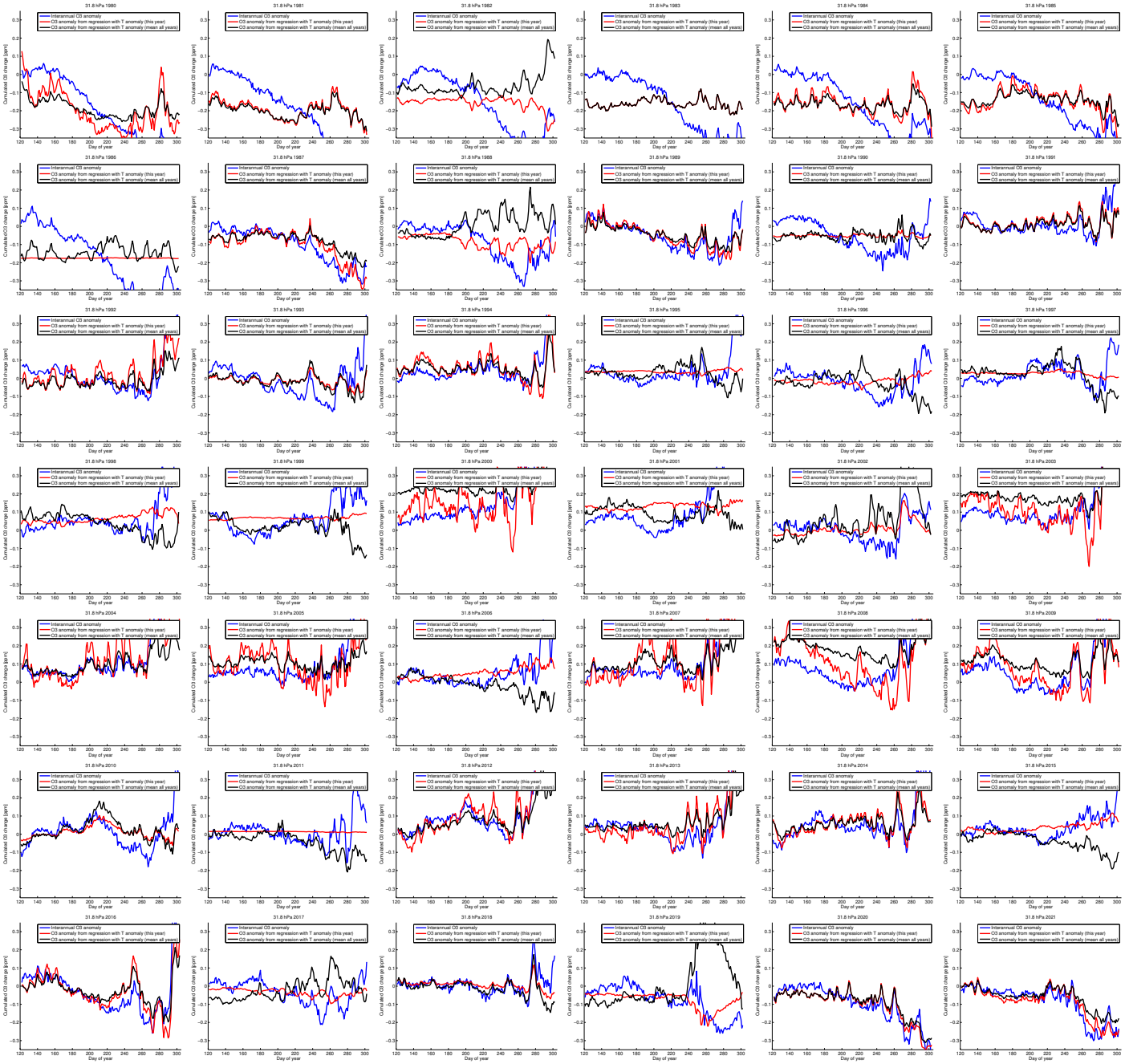

Figure S47: Anomaly of the cumulated vortex-averaged ozone change by transport at 32 hPa (layer 4) for the southern hemispheric winters 1980–2021 (blue, after subtraction of the change by transport that is constant in every year), vortex-averaged temperatures of the individual years regressed on the ozone anomaly (red) and vortex-averaged temperatures scaled by the mean slope of the regressions of all years (black) (cf. Figure 3 of the main manuscript).

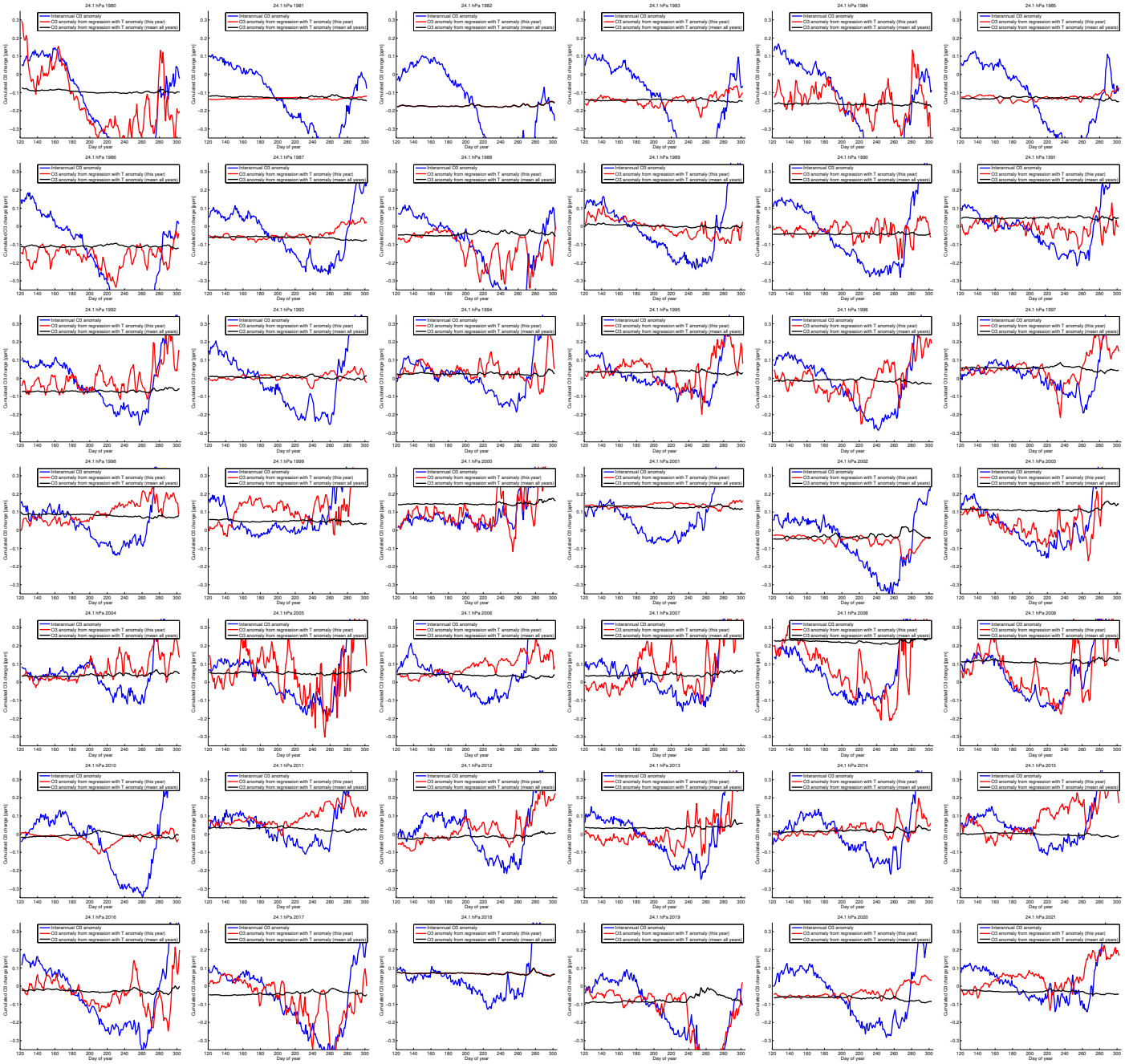

Figure S48: Anomaly of the cumulated vortex-averaged ozone change by transport at 24 hPa (layer 5) for the southern hemispheric winters 1980–2021 (blue, after subtraction of the change by transport that is constant in every year), vortex-averaged temperatures of the individual years regressed on the ozone anomaly (red) and vortex-averaged temperatures scaled by the mean slope of the regressions of all years (black) (cf. Figure 3 of the main manuscript).

13 Vortex mean temperatures (southern hemisphere)

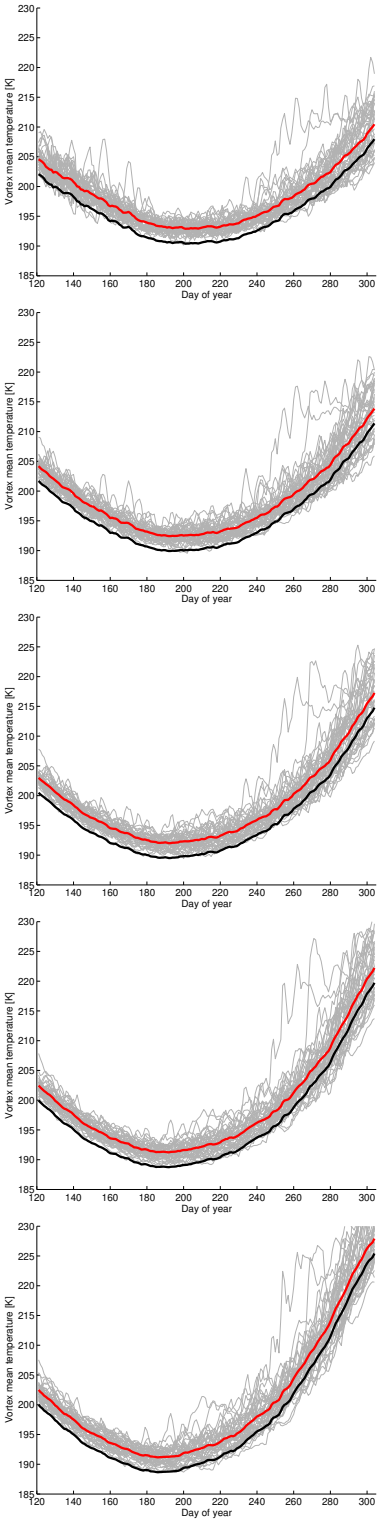

Figure S49: Vortex mean temperatures at the SWIFT levels as a function of day of year for all individual years from 1980 to 2021 based on ERA5 (grey lines), vortex mean temperature averaged over all years (red) and the same curve shifted by $-2.5\,\mathrm{K}$ as an approximation of the lower envelope of the grey lines (black) (cf. Figure 4 of the main manuscript).

14 Validation of the transport term (southern hemisphere)

Figure S50: Cumulated vortex-averaged ozone change by transport at 70 hPa (layer 1) for the southern hemispheric winters 1980–2021 (blue) and a simulation of the cumulated change by transport by a stand-alone version of the transport parameterization (red). The thin grey line shows a simulation with only the constant term, and the thin black line shows a simulation with the constant and temperature-dependent term, but without subtracting the change of the radiative equilibrium temperature from the vortex-averaged temperature change (cf. Figure 5 of the main manuscript).

Figure S51: Cumulated vortex-averaged ozone change by transport at 54 hPa (layer 2) for the southern hemispheric winters 1980–2021 (blue) and a simulation of the cumulated change by transport by a stand-alone version of the transport parameterization (red). The thin grey line shows a simulation with only the constant term, and the thin black line shows a simulation with the constant and temperature-dependent term, but without subtracting the change of the radiative equilibrium temperature from the vortex-averaged temperature change (cf. Figure 5 of the main manuscript).

Figure S52: Cumulated vortex-averaged ozone change by transport at 42 hPa (layer 3) for the southern hemispheric winters 1980–2021 (blue) and a simulation of the cumulated change by transport by a stand-alone version of the transport parameterization (red). The thin grey line shows a simulation with only the constant term, and the thin black line shows a simulation with the constant and temperature-dependent term, but without subtracting the change of the radiative equilibrium temperature from the vortex-averaged temperature change (cf. Figure 5 of the main manuscript).

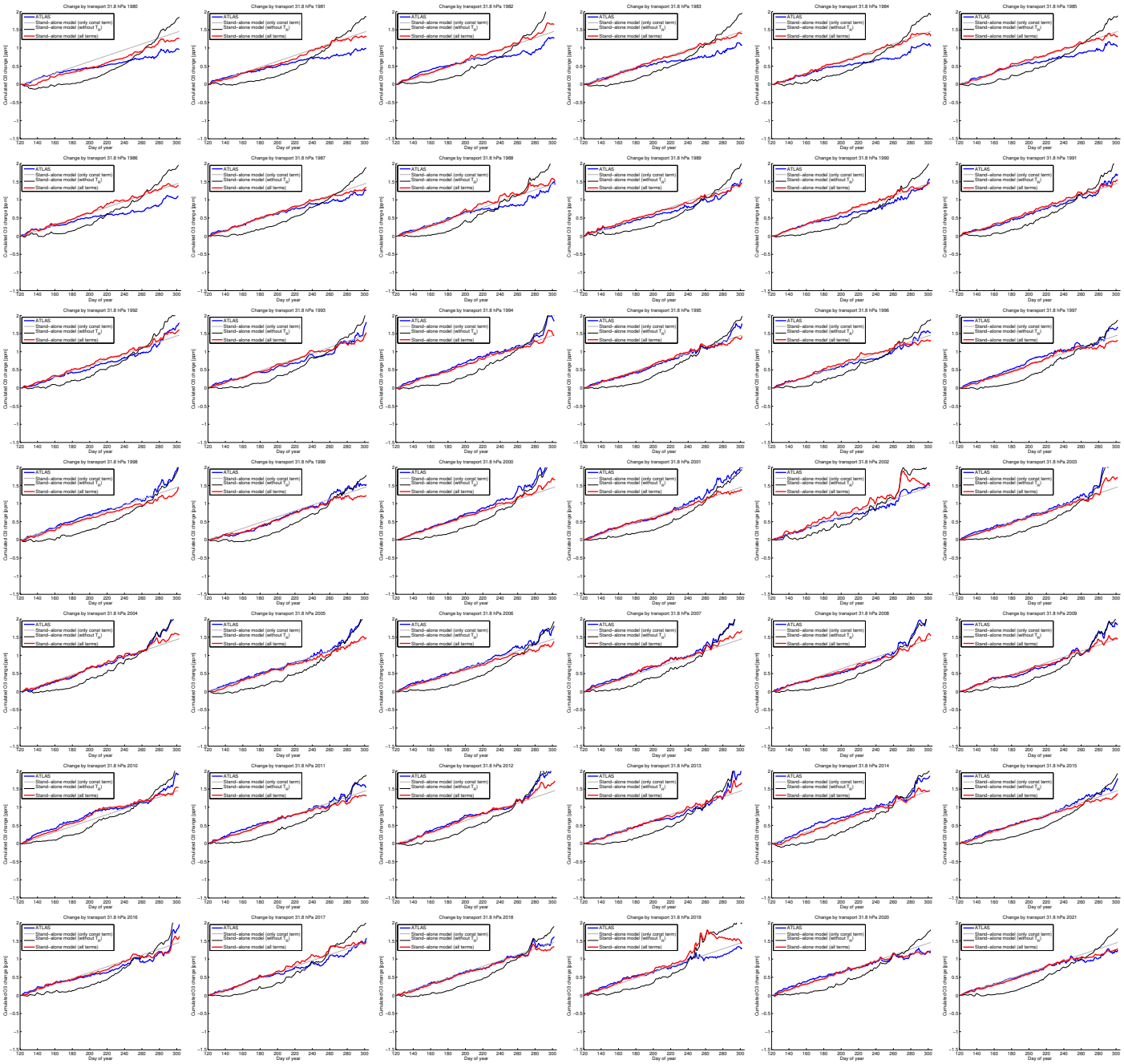

Figure S53: Cumulated vortex-averaged ozone change by transport at 32 hPa (layer 4) for the southern hemispheric winters 1980–2021 (blue) and a simulation of the cumulated change by transport by a stand-alone version of the transport parameterization (red). The thin grey line shows a simulation with only the constant term, and the thin black line shows a simulation with the constant and temperature-dependent term, but without subtracting the change of the radiative equilibrium temperature from the vortex-averaged temperature change (cf. Figure 5 of the main manuscript).

Figure S54: Cumulated vortex-averaged ozone change by transport at 24 hPa (layer 5) for the southern hemispheric winters 1980–2021 (blue) and a simulation of the cumulated change by transport by a stand-alone version of the transport parameterization (red). The thin grey line shows a simulation with only the constant term, and the thin black line shows a simulation with the constant and temperature-dependent term, but without subtracting the change of the radiative equilibrium temperature from the vortex-averaged temperature change (cf. Figure 5 of the main manuscript).

15 Validation of the complete SWIFT model (southern hemisphere)

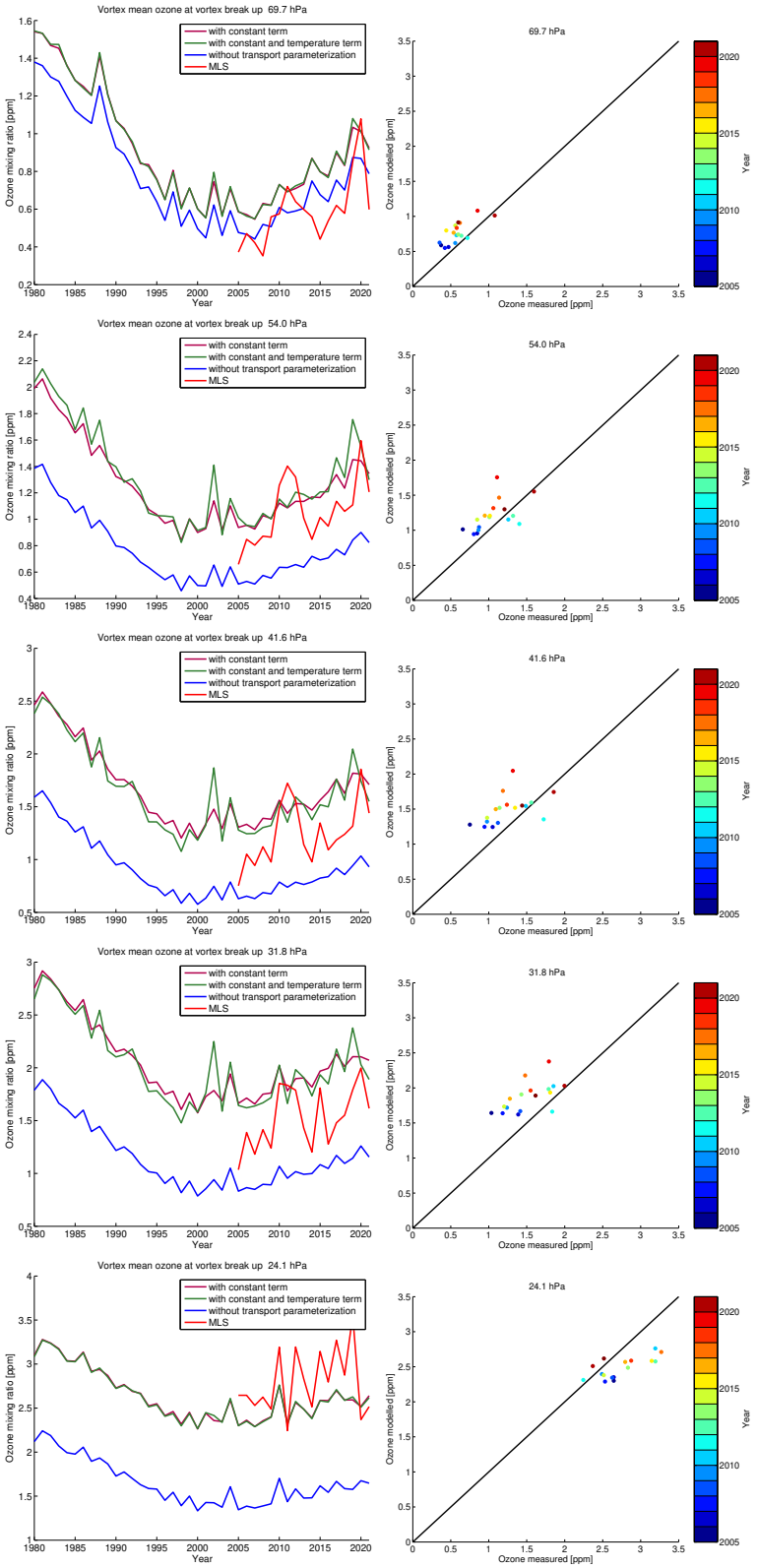

Figure S55: Left (cf. Figure 6 of the main manuscript): Vortex-averaged ozone simulated by the stand-alone Polar SWIFT model for the date of vortex breakup in the southern hemisphere for different years. Ozone mixing ratios simulated without the transport parameterization (blue), ozone mixing ratios simulated with only the "constant change" term of the transport parameterization (brown), ozone mixing ratios simulated with the full transport parameterization with the "constant change" term and temperature-dependent term (green), and corresponding measurements of ozone from the MLS instrument (red). Right (cf. Figure 7 of the main manuscript): Scatter plot of the same data.

16 Difference transport term at vortex breakup of transport parameterization to ATLAS (northern hemisphere)

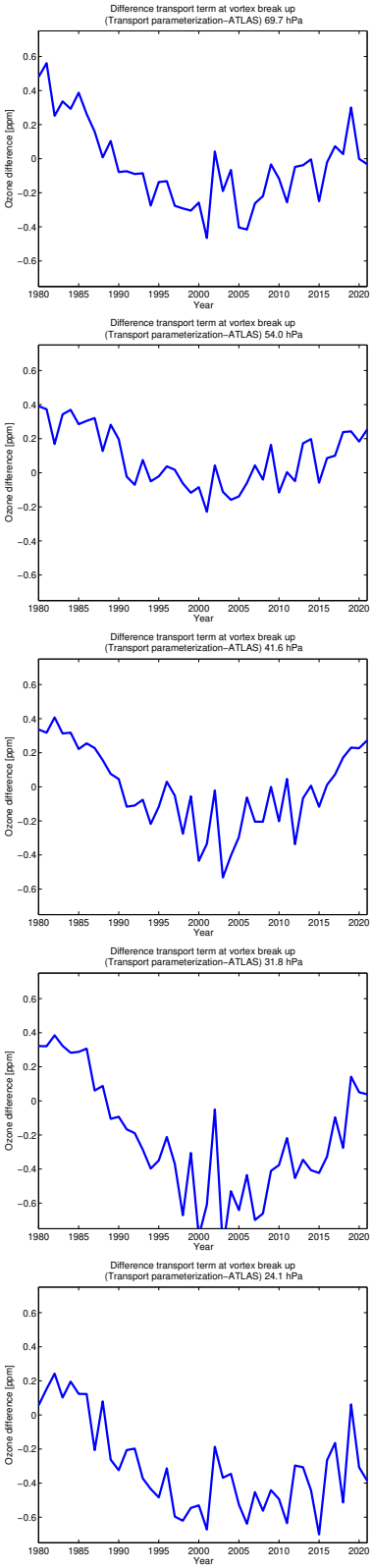

Figure S56: Difference of cumulated vortex-averaged ozone change by transport at vortex break up between the transport parameterization and ATLAS-SWIFT for the southern hemispheric winters 1980–2021.